magnetochemistry

MDPI

*Review*

# Probing Small-Angle Molecular Motions with EPR Spectroscopy: Dynamical Transition and Molecular Packing in Disordered Solids

**Sergei A. Dzuba** [1,2]

[1] Voevodsky Institute of Chemical Kinetics and Combustion, Russian Academy of Sciences, 630090 Novosibirsk, Russia; dzuba@kinetics.nsc.ru
[2] Department of Physics, Novosibirsk State University, 630090 Novosibirsk, Russia

**Abstract:** Disordered molecular solids present a rather broad class of substances of different origin—amorphous polymers, materials for photonics and optoelectronics, amorphous pharmaceutics, simple molecular glass formers, and others. Frozen biological media in many respects also may be referred to this class. Theoretical description of dynamics and structure of disordered solids still does not exist, and only some phenomenological models can be developed to explain results of particular experiments. Among different experimental approaches, electron paramagnetic resonance (EPR) applied to spin probes and labels also can deliver useful information. EPR allows probing small-angle orientational molecular motions (molecular librations), which intrinsically are inherent to all molecular solids. EPR is employed in its conventional continuous wave (CW) and pulsed—electron spin echo (ESE)—versions. CW EPR spectra are sensitive to dynamical librations of molecules while ESE probes stochastic molecular librations. In this review, different manifestations of small-angle motions in EPR of spin probes and labels are discussed. It is shown that CW-EPR-detected dynamical librations provide information on dynamical transition in these media, similar to that explored with neutron scattering, and ESE-detected stochastic librations allow elucidating some features of nanoscale molecular packing. The possible EPR applications are analyzed for gel-phase lipid bilayers, for biological membranes interacting with proteins, peptides and cryoprotectants, for supercooled ionic liquids (ILs) and supercooled deep eutectic solvents (DESs), for globular proteins and intrinsically disordered proteins (IDPs), and for some other molecular solids.

**Keywords:** spin labels and probes; electron spin echo; molecular glasses; supercooled liquids; gel-phase lipid bilayers; intrinsically disordered proteins; ionic liquids



**Citation:** Dzuba, S.A. Probing Small-Angle Molecular Motions with EPR Spectroscopy: Dynamical Transition and Molecular Packing in Disordered Solids. *Magnetochemistry* **2022**, *8*, 19. https://doi.org/10.3390/magnetochemistry8020019

Academic Editors: Angeliki Giannoulis and Dinar Abdullin

Received: 28 December 2021
Accepted: 24 January 2022
Published: 27 January 2022



## 1. Introduction

Organic and biological solids with a disordered molecular structure are interesting from points of view of their practical importance and their unusual fundamental properties. Amorphous polymers [1], materials for photonics and optoelectronic applications [2], and amorphous pharmaceutics [3] possess various advantages compared to their crystalline counterparts: good processability, transparency, uniform physical properties. Biological media always contain disordered fragments [4]. Frozen biological systems are interesting (i) in relation to the problem of cryopreservation of biological tissues; (ii) because of the application of high-resolution spectroscopic techniques carried out at cryogenic temperatures; and (iii) because studies of biological systems at low temperatures may allow an understanding their structure–function relationship, which would be useful to dissect out specific dynamic and structural features that are inevitably also present at higher physiological temperatures.

From a fundamental point of view, disordered molecular solids possess many intriguing properties of a nature that still remains unclear. For example, these media show anomalous thermal conductivity and a specific heat at cryogenic temperatures [5–7]. This

anomaly may be described within a model of tunneling localized excitations or Two-Level Systems model (TLSs) [8–10], in which it is postulated that some atoms or groups of atoms have two equilibrium positions between which they can tunnel [7]. Amorphous solids exhibit also an excess of low-energy vibrational excitations, which is called Boson peak [11,12]. These and other properties are described only at a phenomenological level; for the recent development of theoretical concepts here, see, e.g., reviews [13,14].

For our further narrative, it is helpful also to mention a so-called "Soft Potential Model" [14–18]. This model assumes importance of cubic and quartic terms in Taylor expansion for the potential energy of the molecule near its equilibrium position in the solid. Assuming that the potential $U(q)$ for some selected molecules in the cage formed by its surrounding ($q$ is some generalized coordinate for the molecule) attains a minimum at $q = q_0$, we can write:

$$U(s) = U_0 + \frac{1}{2}b_2 s^2 + \frac{1}{3!}b_3 s^3 + \frac{1}{4!}b_4 s^4 + O(s^5), \quad (1)$$

where $s = q - q_0$, $U_0 = U(q_0)$.

In Figure 1 the potential well given by Equation (1) is schematically depicted as a function of the variable $s$. The motions within the well with hard boundaries (Figure 1a) are restricted dynamical motions, occurring in a periodic way with high frequency (typically in the THz range). In this review, only orientational motions are considered; small-angle dynamical reorientations of the molecules we refer to here as dynamical (molecular) librations. (Although, other terms are sometimes used—e.g., rattling in a cage [19].)

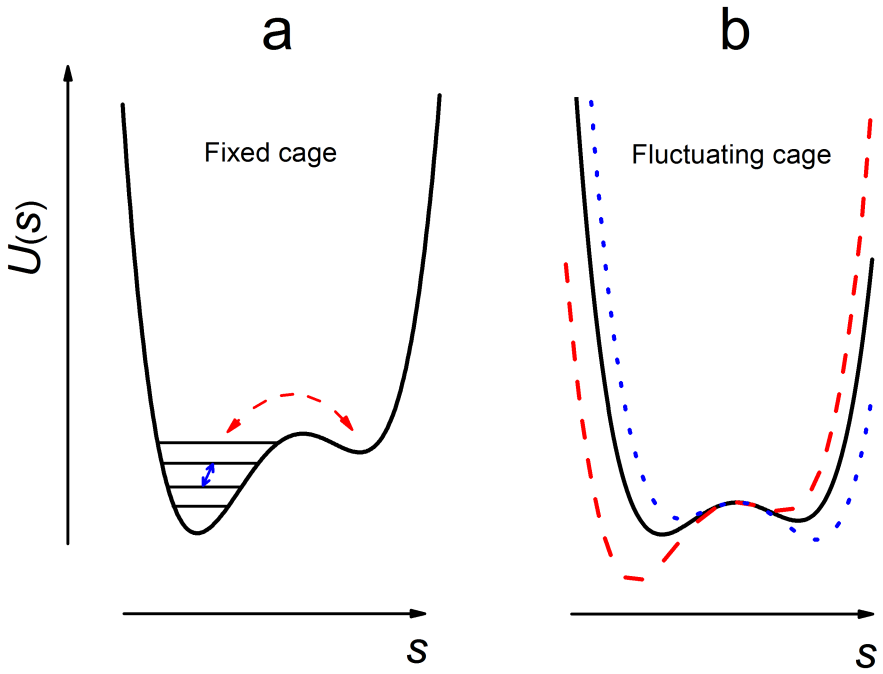


**Figure 1.** Schematic presentation of molecular motions in a solid, described by a generalized coordinate $s$—see Equation (1)—for the molecule captured in a cage formed by its nearest surrounding. (**a**) At low temperatures, the cage is fixed so that only dynamical periodic motion occurs. However random jumps between vibrational level in anharmonic well (small solid arrow) or between nearby shallow wells (curved dashed arrow) results in stochasticity of the motion. (**b**) At higher temperatures, the cage fluctuates and another source of motional stochasticity appear.

Because of the weakness of intermolecular interactions in molecular solids, the cage boundaries may fluctuate (Figure 1b), especially at temperatures close to glass transition temperature ($T_g$). These fluctuations provide a source of stochasticity of motion, so librations may become stochastic. Stochasticity may appear also for random transitions

between vibrational levels in an anharmonic potential, for which the mean amplitude, <*s*>, is a non-zero fluctuating value (Figure 1a, the small solid arrow). Another source of stochasticity could be random jumps between two or more closely spaced shallow wells (Figure 1a, the curved arrow). Small-angle stochastic reorientations of the molecules are here called stochastic (molecular) librations. Furthermore, these motions may be called wobbling motion [20], or quasi-librations [21,22].

Of course, all these hypothetical situations may take place simultaneously, and it is clear that above $T_g$ these intermolecular potentials are destroyed.

Closer to $T_g$, molecular solids transform into supercooled liquids, for which also unusual phenomena are known: secondary Johari–Goldstein $\beta$-relaxation seen in dielectric relaxation [23–26], dynamical transition in neutron scattering and Mössbauer absorption [19,27–29], cooperativity of motions and nanoscale heterogeneity [30,31], and others. The phenomenon of secondary $\beta$-relaxation was also addressed by NMR [32,33]. Some theoretical aspects of supercooled liquids may be described with idealized "mode-coupling theory" [34].

Structure and intrinsic dynamics of molecular glass solids, supercooled liquids and biological systems are extensively explored by different experimental and computational methods. Except for the above-mentioned dielectric and NMR spectroscopies, neutron scattering and Mössbauer absorption, these are optical "hole" burning, single-molecule spectroscopy, atomic force microscopy, dynamics of solvation [30,31], X-ray scattering [35], Raman and Brillouin scattering [35,36], and molecular dynamics (MD) simulations [4,35].

Among others, electron paramagnetic resonance (EPR) of spin probes and labels can also be applied to study the structure and dynamics of disordered media, in its versions of conventional continuous wave (CW) EPR [37] and of more advanced pulsed EPR—electron spin echo (ESE)—spectroscopy [20,38–40].

In spite of the huge amount of literature in the field, the problem with a comprehensive theoretical description of the structure and dynamics of molecular disordered media still remains unsolved. Nevertheless, useful phenomenological models for the molecular packing and motions can be developed. First of all, in solids, molecular motions are restricted in a cage formed by the nearest molecular surrounding, which forms a well potential, as shown in Figure 1, and so only restricted vibrational or small-angle orientational (librational) motions may exist. Second, because of the weakness of intermolecular bonds in molecular solids, it is reasonable to consider this potential as smooth and essentially anharmonic. Finally, also because of the weakness of intermolecular bonds, the well potential may fluctuate stochastically, and stochasticity may appear also because of random transitions between anharmonic sublevels.

## 2. Methodology

### *2.1. CW EPR Spectra of Nitroxides in Molecular Glasses*

EPR spectroscopy of spin labels and probes [41], because of anisotropic character of $g$-tensor and hyperfine interactions, is sensitive to orientational molecular motion. CW EPR is widely employed for obtaining rotational correlation times, in the timescale lying between $10^{-7}$ s and $10^{-10}$ s, for studying anisotropy of the motion, for elucidating its heterogeneity. In solids, unrestricted rotations, however, are suppressed and only small-angle motions (librations, wobbling, etc.) exist.

Nitroxide spin probes may be of different structures, possessing the common paramagnetic $\mathrm{N}-\overset{\bullet}{\mathrm{O}}$ fragment (the unpaired electron is approximately equally distributed between N and O atoms). Two examples are shown in Scheme 1.

The spin Hamiltonian of a nitroxide spin label at the EPR X-band may be taken as [41,42]

$$\hat{H} = \beta \mathbf{B}_{ext} \mathbf{g} \mathbf{S} + g_e \beta \mathbf{S} \mathbf{A} \mathbf{I} \quad (2)$$

where $\beta$ is the Bohr magneton, $\mathbf{B}_{ext}$ the external magnetic field, $\mathbf{g}$ is the $g$-tensor, $g_e$ is the $g$-factor of free electron, $\mathbf{A}$ is the hyperfine interaction (*hfi*) tensor for interaction with a

nitrogen nucleus, expressed in the magnetic field units. Nuclear Zeeman and quadrupole interactions are here neglected because of their smallness. The laboratory framework typically used suggest that the z axis is directed along the magnetic field $\mathbf{B}_{ext}$, when an alternative magnetic field with the microwave frequency $\omega$ is also applied to the system, the solution of Hamiltonian (2) results in the EPR line positions:

$$B_{ext} \equiv B_m(\theta, \varphi) = \frac{\hbar\omega}{\beta g_{zz}(\theta, \varphi)} - ma(\theta, \varphi), \tag{3}$$

where $a(\theta, \varphi) = \sqrt{A_{xz}^2 + A_{yz}^2 + A_{zz}^2}$, and $m$ is the nitrogen nucleus spin projection onto its quantization axis. For $^{14}$N $m$ acquires three values, $-1$, 0, 1.

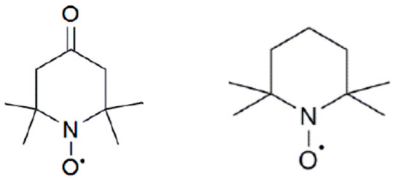


tempone tempo

**Scheme 1.** Chemical structures of nitroxide spin probes tempone and tempo.

Note that in the angular frequency units the $\gamma a(\theta, \varphi)$ value ($\gamma$ is the gyromagnetic ratio) for nitroxides typically is of the order of $10^8$ rad/s. This is a measure of spectral anisotropy that is an essential value for analyzing motions detected by CW and pulsed EPR.

EPR spectra of nitroxide spin labels in solids are determined by anisotropy of the *g*-factor and *hfi* tensors and by the nitrogen spin projection $m$. Three $m$ values result in three hyperfine structure components, broadened in solids due to the anisotropy of magnetic interactions. Also, additional line broadening induced by unresolved *hfi* with nearby nuclei exists. Then $B_{ext}$ is not equal to $B_m(\theta,\varphi)$ that is given by Equation (3), and in polyoriented media the EPR lineshape $g(B_{ext})$ is determined by averaging over all angles $\theta$ and $\varphi$:

$$g(B_{ext}) = \sum_{m=-1}^{1} \frac{1}{4\pi} \iint \sin\theta d\theta d\varphi f(B_{ext} - B_m(\theta, \varphi)), \tag{4}$$

where function $f(B)$ describes this additional broadening induced by unresolved *hfi* with nearby nuclei. In simulations, $f(B)$ usually is approximated by a convolution of Gaussian and Lorentzian lineshapes. The typical result of these simulations is given in Figure 2. The insert in Figure 2 shows the NO paramagnetic fragment and the directions of the molecular axes: the Z molecular axis is assumed to be directed along the axis of the unpaired *p*-electron, the X axis is along the NO bond of the nitroxide, and the Y axis is perpendicular to both. One can see that two side components ($m = \pm 1$) are essentially broadened—because of anisotropy of magnetic interactions—while the central component ($m = 0$) is almost isotropic.

Conventional CW EPR spectra are sensitive to librations because of partial averaging of the parameters of magnetic interaction. Stochastic molecular librations result also in spin relaxation, which can be probed in pulsed EPR, in its version of ESE spectroscopy: spin relaxation induces ESE signal decay. Stochastic molecular librations in the schematic presentation of Figure 1 appear for the cases of a fluctuating surrounding cage and/or fluctuating transitions between vibrational levels in anharmonic potential. Note that random transitions in harmonic potential can hardly induce spin relaxation, because of the high frequency of librational motions (assessed as ~$10^{12}$ $s^{-1}$ [43]).

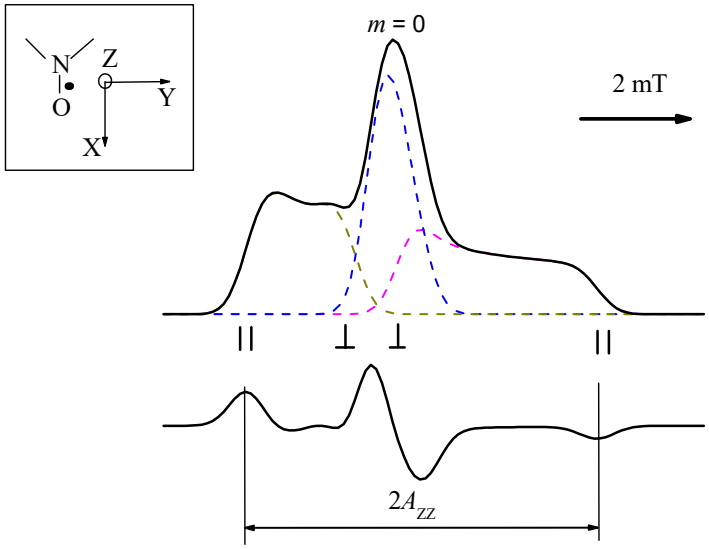


**Figure 2.** CW EPR spectrum of nitroxide calculated by Equation (4) (**top**) and its first derivative, as it is recorded by CW EPR spectrometers (**bottom**). The dashed lines correspond to the spectra for each of three $m$ values. Insert shows the NO paramagnetic fragment and directions of molecular axes; the spectral positions for $m = \pm 1$ corresponding to the Z axis parallel and perpendicular to the magnetic field $\mathbf{B}_{ext}$ are indicated.

### *2.2. CW EPR: Dynamical Librations*

For a librating molecule, Hamiltonian (2) depends on time $t$ and may be separated into the time-independent part, $\hat{H}_0 \equiv < \hat{H}(t) >$ and the time-dependent one, $\Delta\hat{H}(t) = \hat{H}(t) - \hat{H}_0$, where the angular brackets means the average taken over the motion. In the first order perturbation theory,

$$\hat{H}_0 = \beta < g_{zz}(t) > B_{ext} S_z + g_e \beta S_z \ < \mathbf{a}(t) > \mathbf{I}, \tag{5}$$

where the vector $\mathbf{a}(t) \equiv [A_{zx}(t), A_{zy}(t), A_{zz}(t)]$ is introduced. Its averaging we denote as

$$\mathbf{a}_0 \equiv < \mathbf{a}(t) > = [< A_{zx}(t) >, < A_{zy}(t) >, < A_{zz}(t) >]. \tag{6}$$

We denote $A_{XX}$, $A_{YY}$, and $A_{ZZ}$ as the principal values of the *hfi* tensor. Let librational motion occur for simplicity via rotations around the X molecular axis, and let $\alpha(t)$ be the instant small deviation angle ($\alpha^2(t) << 1$) for the motion from the equilibrium position (see Figure 3). Then the new motion-averaged principal values are [42]:

$$\begin{aligned} &< A_{XX} > \equiv A'_{XX} = A_{XX} \\ &< A_{YY} > \equiv A'_{YY} = A_{YY} + (A_{ZZ} - A_{YY}) < \alpha^2(t) > \\ &< A_{ZZ} > \equiv A'_{ZZ} = A_{ZZ} - (A_{ZZ} - A_{YY}) < \alpha^2(t) > \end{aligned} \tag{7}$$

(Note that the tensor trace does not change upon motion, as it must be expected in this case). The analogous relation is valid for the $g$-tensor principal values, if the axes of the two tensors coincide. For motion around the other principal axes, the subscripts in Equation (7) are to be permuted accordingly.

Detailed simulations based on Equations (4) and (7) were performed in [44] for nitroxides in water-glycerol glass; the results showed good agreement with the experiment. In these simulations, all the motion-averaged principal values, $A'_{XX}$, $A'_{YY}$ and $A'_{ZZ}$, were obtained. Below 200 K (that is close to $T_g$), all of them depended linearly on temperature $T$. This linearity may be ascribed to harmonic oscillations for which the relation is expected:

$$\frac{1}{2} I \Omega_{libr}^2 < \alpha(t)^2 > = \frac{1}{2} kT \tag{8}$$

where $I$ is the moment of inertia of the molecule, $\Omega_{libr}$ is the librational frequency in angular units. In combination with Equation (7), Equation (8) indeed provides a linear temperature dependence of the *hfi* values.

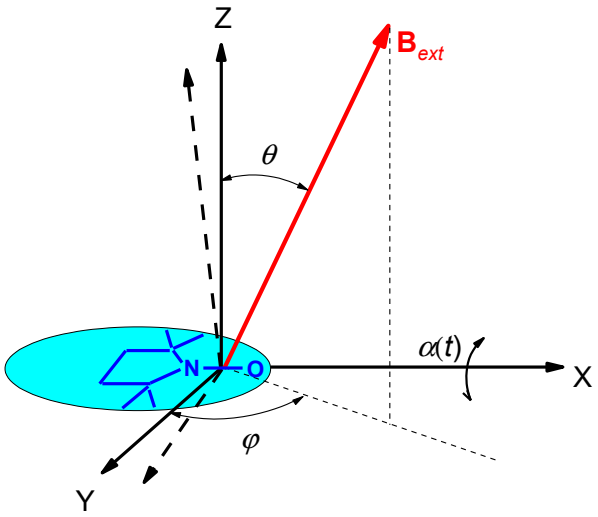


**Figure 3.** The molecular framework of the spin label molecule and its reorientation around the X molecular axis by an angle $\alpha(t)$. Direction of the magnetic field $\mathbf{B}_{ext}$ is determined by the angles $\theta$ and $\varphi$ in the equilibrium framework (for $\alpha = 0$).

It is interesting to note also that the slopes of the straight lines determined in [44] for different molecular glass formers were found to correlate with the "fragility" [45] of the glass, see also the discussion below, in Section 4.9.

At low temperatures, the thermal energy of librating molecules is comparable with the elementary quantum, so the onset of quantum effects is expected. Then $< A_{XX} >$ will be determined by the Bose factor $n(\Omega) = 1/(\exp(\hbar\Omega/kT) - 1)$:

$$< A_{XX} >= A_{XX} + (A_{YY} + A_{ZZ} - 2A_{XX})\frac{\hbar}{I\Omega_{libr}}\left\{\frac{1}{\exp(\hbar\Omega_{libr}/kT) - 1} + \frac{1}{2}\right\}. \quad (9)$$

When $kT > \hbar\Omega_{libr}$, $<A_{XX}>$ linearly depends here on a temperature that is in line with Equation (8).

In [43], the motion-averaged $<A_{XX}>$ principle values were measured at cryogenic temperatures by a pulsed electron-nuclear double resonance (ENDOR) technique for $^{15}$N-substituted nitroxides. The results are given in Figure 4 for glycerol and o-terphenyl glasses, along with the $<A_{ZZ}>$ principle values found from the splitting between the two outmost spectral components (cf. Figure 2). The fitting of $<A_{XX}>$ temperature dependence allowed to assess the $\Omega_{libr}/2\pi$ value as 60 cm$^{-1}$ for glycerol and 90 cm$^{-1}$ for o-terphenyl. This result coincided fairly well with the Raman scattering data also obtained for these glasses [43], which showed that dynamical librations of guest nitroxide molecules is determined by the vibrations of the host molecules. The similar results were also obtained for glassy liquid crystals [46].

Note that above 80 K in glycerol and above 112 K in o-terphenyl the $<A_{XX}>$ temperature dependences in Figure 4 manifest a kink with a slope slightly smaller at higher temperatures. The reason for this kink is not clear. It is likely a result of influence of anharmonicity of the motion, which may become essential at higher temperatures—up to the overcoming of one of the barriers in the potential well (see Figure 1a).

Therefore, CW EPR spectra of guest spin probes in molecular glasses provide information on mean squared amplitude $< \alpha(t)^2 >$ of dynamical librations. The $< \alpha(t)^2 >$ value may directly obtained from the experimental data in Figure 4, employing Equations (7), (8) or (9); it attains maximal value of ~0.1 rad$^2$.

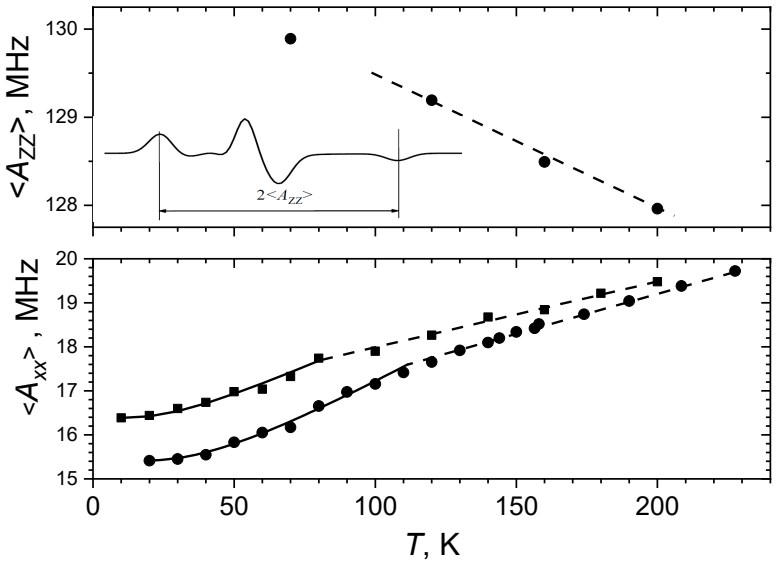


**Figure 4.** The $<A_{ZZ}>$ values (**top**) obtained from CW EPR spectra (see insert) and the $<A_{XX}>$ values obtained from the $^{15}$N-ENDOR peak positions (**bottom**) for the $^{15}$N-substituted nitroxide spin probe in *o*-terphenyl (circles) and in glycerol (squares) glasses. Solid lines present fitting employing Equations (7) and (9). Dashed lines are linear dependences at high temperatures (see text), which follows Equations (7) and (8). Adapted with permission from [43], American Institute of Physics.

### *2.3. ESE: Stochastic Librations*

In ESE spectroscopy—a pulsed version of EPR—an echo signal appearing after application of several microwave pulses on an electron spin system in the magnetic field is studied. The microwave frequency is the EPR resonance frequency. The simplest pulse ESE sequence contains only two pulses, with the 90° and 180° magnetization turning angles, and is denoted as 90°–$\tau$–180°–$\tau$–*echo detection*, where $\tau$ is the time delay between pulses. The echo signal time dependence, $E(2\tau)$, decays with a $2\tau$ increase because of spin relaxation.

Spin relaxation appears because of stochastic fluctuations of magnetic interactions, and stochastic molecular motion provides an important source of these fluctuations. For nitroxide spin probes dissolved in molecular glasses, spin relaxation induced by molecular motion in molecular glasses was first detected with ESE in [38–40], and these ESE-detected motions in molecular glasses were then ascribed to stochastic molecular librations [47,48].

The assignment [47,48] to stochastic molecular librations was performed on the following basis. Microwave pulses normally employed in ESE spectrometers excite only a small portion of the EPR spectrum. In solids, different EPR spectral positions correspond to different orientations of nitroxide (see Figure 2), and these positions possess a different degree of anisotropy of magnetic interactions. Then for restricted small-angle motion the EPR spectral positions with a larger spectral anisotropy are characterized by a faster ESE decay, which is indeed observed in experiment.

Figure 5 shows echo-detected EPR spectra (the spectra obtained as an echo signal intensity taken upon the scanning magnetic field) for nitroxide tempone in glycerol glass at different time delays $\tau$, at two different temperatures (200 and 216 K) [49]. The spectra are normalized by their central peak amplitude, which excludes from consideration all field-independent spin-relaxation mechanisms. One can see in Figure 5 that, first, the echo signal decays with a $\tau$ increase faster for low- and high-field hyperfine components, making these components lower in amplitude. These components are essentially anisotropic, and so this relaxation rate enhancement may indeed be ascribed to the orientational motion. Second, relaxation at the middle of these two components is faster compared with two outer shoulders of the spectrum. Third, intensity of the spectral position 2 decays exponentially with time $\tau$, as it is seen in the insert. As the zero time $\tau$ cannot be achieved in experiment

because of the ESE spectrometer dead time problem, the spectral intensity for $\tau$ = 0 for both temperatures 200 and 216 K in Figure 5 is ascribed to that at the reduced temperature of 181 K, where the motions may be assumed to be frozen out (at time $\tau$ =136 ns that is the starting $\tau$ delay after the dead time).

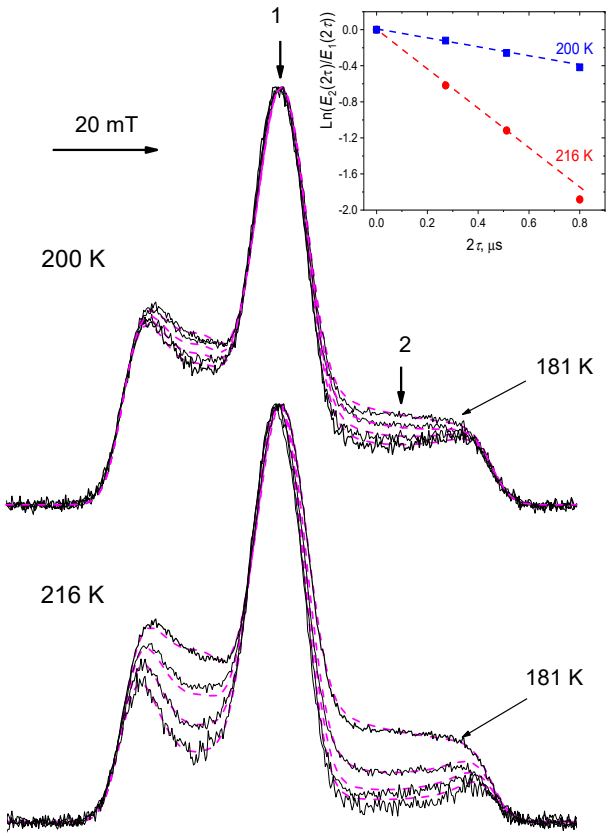


**Figure 5.** Echo-detected EPR spectra normalized by their maximal intensity, for nitroxide tempone in glycerol glass at temperatures 200 K and 216 K ($\tau$ sequentially equals 136, 256 and 400 ns). Dashed lines present simulations for the model of stochastic molecular librations (see text). The insert shows time dependence of the $\ln(E_2(2\tau)/E_1(2\tau))$ value for the field positions 1 and 2 indicated by arrows in the main figure, this value at $\tau$ = 0 is assumed to be determined by that at $\tau$ = 136 ns for 181 K (it is then subtracted). Adapted with permission from [49], Springer.

These three features of manifestation of spin relaxation seen in experimental spectra in Figure 5 can be readily explained theoretically within the librational model. We consider here the case of small-amplitude motions, resulting in spectral diffusion within the excitation bandwidth only. The general expression for the echo signal $E(2\tau)$ then is given by the relation [50]:

$$E(2\tau) \propto < \exp\left(-i\int_0^{\tau} dt\Delta\omega(t)\right)\exp\left(i\int_{\tau}^{2\tau} dt\Delta\omega(t)\right) >, \quad (10)$$

where $\Delta\omega(t) = \frac{1}{\hbar}(<1\left|\hat{H}(t) - \hat{H}_0\right|1> - <2\left|\hat{H}(t) - \hat{H}_0\right|2>)$, and 1 and 2 denote two electron spin states of the unperturbed Hamiltonian $\hat{H}_0$—see Equation (5). If spectral diffusion due to stochastic motions is fast (correlation time of the motion $\tau_c << \tau$), and occurs via random walks within a restricted frequency interval, Equation (10) results in an exponential decay [50,51]:

$$E(2\tau) \propto \exp(-2\tau < \Delta\omega^2(t) > \tau_c). \quad (11)$$

Note that for restricted small-angle librations one may assume that $< \Delta\omega^2(t) >$ exists. Also note that the condition $\tau_c << \tau$ of fast motion may be alternatively presented as [50,51]

$$< \Delta\omega^2(t) > \tau_c^2 << 1 \quad (12)$$

(the so-called limit of Redfield's theory of spin relaxation).

Let us consider reorientation by small angle $\alpha(t)$ around the X molecular axis—see Figure 3. For nitroxides, $\Delta\omega(t)$ depends also on the angles $\theta$ and $\varphi$ determining the orientation of the magnetic field in the molecular framework (see Figure 3). For $\alpha^2(t) << 1$ we may write [52,53]:

$$\Delta\omega(t, \theta, \varphi) = \alpha(t) R_X(\theta, \varphi, m) \quad (13)$$

with

$$R_X(\theta, \varphi, m) = [\frac{\beta}{\hbar} B_{ext}(g_{YY} - g_{ZZ}) + \frac{m(A_{YY}^2 - A_{ZZ}^2)}{\sqrt{A_{XX}^2 \sin^2\theta\cos^2\varphi + A_{YY}^2 \sin^2\theta\sin^2\varphi + A_{ZZ}^2\cos^2\theta}}] \sin\theta\cos\theta\sin\varphi \quad (14)$$

For motion around the Y molecular axis, the $(g_{YY} - g_{ZZ})$, $(A_{YY}^2 - A_{ZZ}^2)$ and $\sin\theta\cos\theta\sin\varphi$ factors are to be replaced correspondingly by the $(g_{XX} - g_{ZZ})$, $(A_{XX}^2 - A_{ZZ}^2)$ and $\sin\theta\cos\theta\cos\varphi$ ones. If magnetic tensors are (nearly) axially symmetrical, the motion around the Z molecular axis does not result in spin relaxation.

If the reorientation angle $\alpha(t)$ is small, angles $\theta$ and $\varphi$ in Equations (13) and (14) may be considered as constants. The nitrogen nuclear spin projection $m$ in principle also fluctuates upon motion, because of fluctuation of hyperfine interaction. This fluctuation would result in large-scale spectral diffusion between three hyperfine structure components, which may be directly monitored by a magnetization transfer experiment in double electron-electron resonance technique [54–56]. However, these experiments have shown that the nitrogen nuclear spin relaxation rate $W_N$ is of the order or less than $10^5$ s$^{-1}$, which is much smaller than the rate of echo decay in organic solids that is typically larger than $10^6$ s$^{-1}$ (cf. Figure 5). Therefore, nitrogen nuclear relaxation in nitroxides normally may be neglected then analyzing the spin relaxation induced by stochastic molecular librations, and $m$ in Equation (14) may be considered as a constant.

Equations (11) and (13) for the motion around the X molecular axis result in the expression

$$E(2\tau) \propto \exp(-2\tau R_X^2(\theta, \varphi, m) < \alpha^2(t) > \tau_c). \quad (15)$$

If one assumes the axial symmetry for the nitroxide $g$- and hfi tensors, so that $A_{XX} = A_{YY} \equiv A_\perp, A_{ZZ} \equiv A_{||}$ (with the analogous expressions for the g-tensor), then Equation (14) reduces to

$$R_X(\theta, \varphi, m) = \gamma[B_{ext}(g_\perp - g_{||}) + m(A_\perp^2 - A_{||}^2)/a_0] \sin\theta\cos\theta\sin\varphi \quad (16)$$

For the echo-detected EPR lineshape, $g_{ED}(B_{ext}, 2\tau)$, instead of Equation (4) we have:

$$g_{ED}(B_{ext}, 2\tau) = \frac{1}{4\pi} \sum_{m=-1}^{1} \iint \sin\theta d\theta d\varphi f(B_{ext} - B_m(\theta, \varphi)) \times \exp(-2\tau R_X^2(\theta, \varphi, m) < \alpha^2(t) > \tau_c) \quad (17)$$

When comparing experimental ESE signal decay with these theoretical predictions, one has to take into account that except for molecular motion, spin relaxation in solids is induced also by other physical mechanisms: spin relaxation of nearby nuclear and electron spins and spin–spin interactions, spin–lattice relaxation (see [57–61] for more details). Some of these additional mechanisms, however, are too slow to influence the ESE signal decay (spin–lattice relaxation, e.g.,); the others are field-independent (spin relaxation of the nearby spins, e.g.) and so cannot influence the echo-detected EPR lineshapes. The only example of the mechanism which is also field-dependent is the so-called "instantaneous spectral diffusion" [50], see e.g. [62] for description of its manifestation for nitroxides. Fortunately,

this additional mechanism is temperature-independent, and so its contribution may be easily selected at a temperature that is low enough that motions are suppressed. The way that its influence on echo-detected EPR spectra may be eliminated is described in detail in [62]. And this mechanism certainly does not intervene to the echo decays when the spin concentration in the sample is small.

If the echo-detected EPR spectra are normalized by their maxima, all field-independent relaxational mechanisms are excluded from our consideration and the spectral changes observed may be ascribed to stochastic molecular librations (taking in mind only the possible influence of the instantaneous diffusion mechanism). Simulations based on Equations (15)–(17) fitted to experimental spectra are given in Figure 5 by dashed lines. Note that all the spectral parameters are obtained by fitting the CW EPR spectra and only one free fitting parameter is employed here for echo-detected EPR spectra: the $< \alpha^2(t) > \tau_c$ product.

As was said above, the zero-time delay $\tau = 0$ is inaccessible in the experiment because of the ESE spectrometer dead time problem. In simulations, this problem does not exist, and in Figure 6 the results of simulations are presented, starting from $\tau = 0$. The EPR spectral parameters were used: $g_\perp - g_\parallel = 0.0050$, $B_{ext}$ = 3400 G (0.34 T), $A_\parallel = 35$ G, $A_\perp = 5$ G, and an individual Gaussian line broadening was of 3 G. The insert in Figure 6 shows the $\ln(E_2(2\tau)/E_1(2\tau))$ ratio at different delays $2\tau$. One can see that this ratio depends almost linearly on $2\tau$:

$$E_2(2\tau)/E_1(2\tau) \cong const\ \exp(-2\tau\Delta W) \quad (18)$$

where $\Delta W$ may be referred to as an anisotropic relaxation rate experimentally obtained using this approximation. This dependence in principle follows from the theoretical Equation (11), which however, is to be averaged over the different angles $\theta$ and $\varphi$.

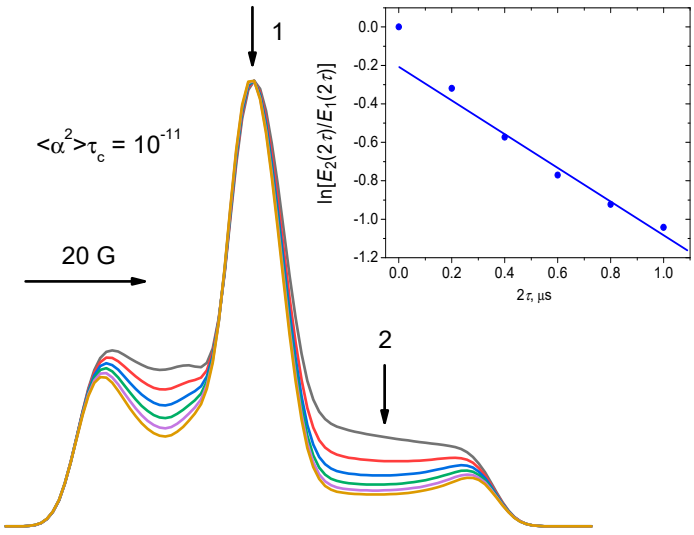


**Figure 6.** Simulations employing Equations (15)–(17), for the spectra normalized by their maximal amplitude. The EPR spectrum parameters are given in the text. The $< \alpha^2(t) > \tau_c$ parameter is $10^{-11}$ rad$^2$s, and $2\tau$ acquires the sequential values of 0, 0.2, 0.4, 0.6, 0.8 and 1 μs. The insert shows time dependence of the $\ln(E_2(2\tau)/E_1(2\tau))$ value, with that at $\tau = 0$ subtracted from all the data; the straight line shows a linear approximation for $2\tau > 0$

The tangent in insert to Figure 6 is equal to ~$0.9 \times 10^6$ s$^{-1}$. Comparing Equations (15) and (18), we can write

$$\Delta W = R_{12} < \alpha^2(t) > \tau_c, \quad (19)$$

with the constant $R_{12} = 0.9 \times 10^{17}$ rad$^{-2}$s$^{-2}$.

The alternative mechanism of molecular motion could be unrestricted Brownian orientational diffusion via infinitesimal steps. This mechanism is commonly employed to describe molecular motions in liquids. For this mechanism, unrestricted spectral diffusion

appears (still developing within the excitation bandwidth, otherwise the echo signal will not appear), with echo decaying as [49]:

$$E(2\tau) \propto \exp(-R_X^2(\theta, \varphi, m) D_X \frac{2}{3}\tau^3), \quad (20)$$

where $D_X$ is the diffusion coefficient in the angular space, for motion around the X molecular axis. Note that $R_X(\theta, \varphi, m)$ here plays the role of the field gradient that in the NMR studies of molecular diffusion is applied artificially [51]. However, this mechanism establishes the cubic dependence on the time delay $\tau$ under the exponent, which is not observed in the experiment for molecular solids (cf. Figure 5), which excludes this possibility. However, some admixture of this mechanism may also appear for large time delays $\tau$ [49].

The condition (12) for fast stochastic motion depends on the EPR frequency band. The simulations described here (Figures 5 and 6) refer only to the X-band (microwave frequency ~9 GHz). For high-frequency EPR, this condition may be violated. However, good agreement between theory and experiment was also obtained for Q-band (35 GHz) [63] and for 3, 95 and 180 GHz [64]. On the other hand, high-frequency EPR, because of higher sensitivity to anisotropy, may also probe intermolecular motion [65] instead of the motion of a molecule as a whole, that takes place for X-band EPR. Stochastic molecular librations were detected in high-field EPR also in [66–71].

Note that the result of the $< \alpha^2(t) >$ averaging in Equation (15) for stochastic motion may differ from the analogous averaging in Equation (7) for dynamical librations. Indeed, dynamical librations may be of a very high frequency, lying in the THz region (see above). ESE decays become insensitive to this high-frequency motion, even if these motions are stochastically damped [49]. Then, the amplitude of dynamical librations is determined by the width of the potential well, while for the stochastic process the amplitude is determined by the scale of fluctuation of the well walls, or by fluctuating the $< \alpha(t) >$ value upon the transitions in an anharmonic potential (see Figure 1a,b). The results of these two averaging may be of the same order of magnitude, but they also may be different.

Note also that in addition to the traditional nitroxide spin labels, other types of spin-labeled molecules were found to manifest stochastic molecular librations as well: quinone anions in photosynthetic reaction centers [67–69], triarylmethyl radicals [72], copper complexes [73], transient triplet states appearing upon photoexcitation [74].

### *2.4. Stimulated ESE: Slow Motions*

Stimulated ESE appears after application of three pulses in a sequence 90°–$\tau$–90°–$t_{SE}$–90°–$\tau$–*echo detection*, where $t_{SE}$ is an additional time delay. Stimulated echo is sensitive to motions in the microsecond time scale [20,75] that is determined by the spin-lattice relaxation time, $T_1$. Reorientations by the angles larger than ~2° can be studied by pulse excitation near the canonical orientations of the nitroxide spin probe, at which the spectral anisotropy is small [20]. For pulse excitation at the spectral positions between canonical orientations [75], the anisotropy is high, ~$5 \times 10^8$ rad$\times$s$^{-1}$ at X-band, which for $t_{SE}$ ~$10^{-6}$ s results in the acquired phase around unity for the angle of ~0.1°. The detection of such small-amplitude molecular reorientations is a unique property of the ESE technique.

In the case of small-scale motions, spectral diffusion develops within the pulse excitation band width only, and the echo signal decay in the stimulated echo experiment is described as [50]:

$$E(2\tau + t_{SE}) \propto < \exp\left(-i\int_0^{\tau} dt\Delta\omega(t)\right) \exp\left(i\int_{\tau+t_{SE}}^{2\tau+t_{SE}} dt\Delta\omega(t)\right) >, \quad (21)$$

(cf. Equation (10)); the two-pulse echo formally corresponds to $t_{SE} = 0$.

If stochastic motions are fast ($\tau_c < \tau$), Equation (21) results in an exponential decay [50,51]:

$$E(2\tau + t_{SE}) \propto \exp(-2\tau\tau_c < \Delta\omega^2(t) >), \quad (22)$$

provided that $< \Delta\omega^2(t) >$ exists. It is important to note that the right-hand part here is independent on the $t_{SE}$ delay.

In many applications of spin-label EPR, the mechanism of unrestricted Brownian spectral diffusion via infinitesimal steps in the frequency space is considered [37,38]. If this diffusion is developing within the excitation bandwidth, the echo decays as [51]

$$E(2\tau + t_{SE}) \propto \exp(-D_\omega(\frac{2}{3}\tau^3 + \tau^2 t_{SE})), \quad (23)$$

where $D_\omega$ is the diffusion coefficient in the EPR frequency space. For simplicity, we assume the axial symmetry of the nitroxide $g$- and the hyperfine interaction tensors. For small angles $\alpha(t)$ of motion around the X molecular axis, the relation (13) takes place. Then, instead of (23), we have

$$E(2\tau + t_{SE}) \propto \exp(-R_X^2(\theta, \varphi, m)D_X(\frac{2}{3}\tau^3 + \tau^2 t_{SE})), \quad (24)$$

where $D_X$ is the diffusion coefficient for motion around the X molecular axis in the angular space (cf. with Equation (20)).

Numerical studies on stimulated ESE decays for spin probes in molecular glasses [76–80] have shown, however, that functional dependence on the time delays $\tau$ and $t_{SE}$, instead of Equation (24), is given by the expression:

$$E(2\tau + t_{SE}) \propto \exp(-const_1 \cdot \tau - const_2 \cdot \tau t_{SE}). \quad (25)$$

The inapplicability of Equation (24) here can be easily rationalized because for reorientations within the small angles (0.1°–1°) the model of infinitesimal angular steps may hardly be appropriate. It is reasonable, therefore, to assume that within such small reorientations the molecule freely rotates (the model of free rotational diffusion [81,82]). Denoting the angular velocity of rotation as $\Omega_{rot}$ and $g(\Omega_{rot})$ as its distribution function, from general Equation (21) for this model one obtains [76]:

$$E(2\tau + t_{SE}) \propto \int \cos[R_X(\theta, \varphi, m)\Omega_{rot}(\tau^2 + \tau t_{SE})]g(\Omega_{rot})d\Omega_{rot}, \quad (26)$$

The unique property of this formula is its dependence on the multiplication of the two time delays, $\tau$ and $t_{SE}$, which is in agreement with the experimental observation presented by Equation (25).

For small $t_{SE}$ ($\tau$ is also small, typically $\tau << t_{SE}$), Equation (26) may be expanded in terms of the parameter $|R_m(\theta, \phi)|\Omega_{rot}(\tau^2 + \tau t_{SE})$. Assuming that the distribution $g(\Omega_{rot})$ is normalized, $\int g(\Omega_{rot})d\Omega_{rot} = 1$, the first-order Taylor expansion can be formally presented as

$$E(2\tau + t_{SE}) \propto 1 - |R_m(\theta, \phi)|\Omega_0\tau t_{SE} \approx \exp(-|R_m(\theta, \phi)|\Omega_0\tau t_{SE}) \quad (27)$$

where $\Omega_0$ is a positive value determining the first-order expansion term. The term proportional to $\tau^2$ is omitted here because of its smallness. Note that expansion (27) is valid only when the $g(\Omega_{rot})$ second moment diverges; for the case of the Lorentzian $g(\Omega_{rot})$ distribution, Equation (27) becomes an exact result.

Like in the above case of studying stochastic librations with two-pulse ESE, all isotropic relaxation processes may be discarded by comparing echo decays for the field positions

of different spectral anisotropy. Then, taking into account that stochastic librations also contribute to the echo decay, and combining Equations (15) and (27), we finally write

$$E_2(2\tau + t_{SE})/E_1(2\tau + t_{SE}) = const\ \exp(-2\tau\Delta W_{12} - \tau t_{SE}\Delta S_{12}), \quad (28)$$

where $\Delta S_{12} = \sqrt{R_{12}}\Omega_0$ (cf. Equation (18), Equation (19)), which is in full agreement with the empirical dependence (25). Then, from a linear dependence of the experimental ratio $\ln(E_2(2\tau + t_{SE})/E_1(2\tau + t_{SE}))$ on the time delay $\tau$, one obtains

$$\Delta W_{3-p}(t_{SE}) = 2\Delta W_{12} + t_{SE}\Delta S_{12} \quad (29)$$

as a tangent of this dependence.

Figure 7 presents a typical example of this type of experiment, performed for tempone spin probe in *o*-terphenyl glass [77]. One can see that linear dependences indeed take place, in full agreement with Equation (29). At temperatures below ~259 K the tangent of the slope for these dependences is almost zero. This means that, according to Equation (22), stochastic motions are fast, $\tau_c < \tau$ ($\tau$ is of the order of ~$10^{-7} \div 10^{-6}$ s).

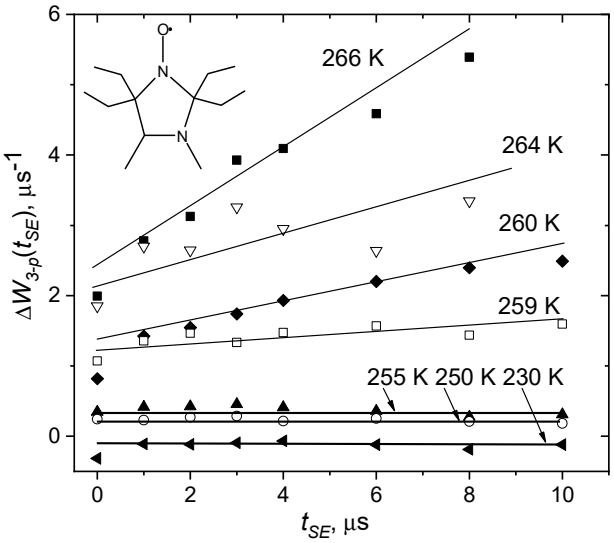


**Figure 7.** Dependence of the $\Delta W_{3-p}(t_{SE})$ relaxation rate (see Equation (29)), obtained in the three-pulse stimulated ESE experiment in *o*-terphenyl glass for nitroxide spin probe shown in the insert. Adapted with permission from [77], Elsevier.

At higher temperatures, the tangent of the slope increases. According to Equations (28) and (29), this tangent is $\Delta S_{12} = \sqrt{R_{12}}\Omega_0$. Then, employing the estimated above value $R_{12} = 0.9\ 10^{17}$ rad$^{-2}$s$^{-2}$, one can obtain the angular velocity $\Omega_0$. From data in Figure 7 it follows that near, say 260 K, $\Omega_0$ is of the order of $10^3$ rad/s. Then, for $t_{SE}$ ~$10^{-5}$ s, we obtain that the reorientation angle is of the order of 1°.

There are two alternative possibilities how to interpret the slow rotations found in this experiment: it may be an independent type of motion appearing at elevated temperatures, or it may be stochastic librations found in the two-pulse experiment, for which the correlation time $\tau_c$ becomes larger than $10^{-7}$ s. (The $\tau_c$ may increase with temperature because of increase of cooperativity of the motion).

Therefore, the three-pulse stimulated ESE experiment allows the detection of slow rotations of spin labels, developing in the microsecond time scale via small angles—typically less than ~1°. If in this experiment the independence of echo amplitude on the time delay $t_{SE}$ is observed, this supports the model of fast stochastic librations, with correlation times $\tau_c$ less than $10^{-7}$ s [75].

## 3. General Features of Small-Angle Motions in Solids

### *3.1. Dynamical Librations and Transition in Molecular Glasses*

Numerous neutron scattering data show that in molecular disordered media dynamical transition appears as a sharp increase of the motional amplitude at a certain temperature, $T_d$. [27–29,83]; a similar effect was observed in a Mössbauer absorption experiment [27,84]. Both these techniques probe mean square displacement of atoms (MSD), $<x^2>$, where $x$ is the individual displacement. Neutron scattering probes the motion of hydrogen atoms. It is sensitive to the motions developing in the picosecond-nanosecond time scale. Mössbauer absorption is sensitive to motions of ferrous atoms naturally presenting in some proteins, or artificially inserted into molecular glass formers. It is sensitive to motions faster than $10^{-7}$ s. For harmonic motions, $<x^2>$ is expected to linearly depend on the temperature, which is indeed observed below $T_d$. Above $T_d$, a drastic enhancement of $<x^2>$ is observed, which is attributed to the onset of anharmonic or diffusive motions. Typically, $<x^2>$ attains a value of ~0.1 Å$^2$.

Dynamical transition was found for simple molecular glass-formers [84–89], small amino acids [90], proteins [27–29,83], DNA and RNA [91], biological membranes [92–95], and also for non-biological polymers [96]. Nowadays, it is assumed to be a general property of disordered and biological environments. In biological systems, $T_d$ lies in the interval from 170 to 230 K. The importance of dynamical transition for proteins is determined by the experimental fact that it can correlate with the onset of protein function [27–29,83].

The background and general atomistic picture of the dynamical transition is still debated. It has been also pointed that the observed effects may appear due to the limited resolution of the experiment when the relaxation time of the system merely enters the instrumental time window [97–102].

Molecular motions result in the CW EPR spectra narrowing, as it was stated above—see Section 2.2 and Figure 4 (top) therein—for the motions in the nanosecond time scale or faster. This time scale is similar to that for the neutron scattering and Mössbauer absorption experiments. Then, for a molecule of the $l \sim 1$ Å size, 0.1 Å$^2$ implies that for reorientation angle $\alpha^2 \sim <x^2>/l^2 \sim 0.1$ rad$^2$, which is in agreement with that found from CW EPR spectra, see the assessments in Section 2.2 and in [103]. Therefore, one may assume that CW EPR should provide results consistent with the neutron scattering and Mössbauer absorption spectroscopies.

This hypothesis can be proved by comparison data in glassy orthoterphenyl obtained by neutron scattering [87,88] and by EPR for spin probe tempone [103]. Figure 8 presents the results of this comparison, for $<x^2>$ and $<\alpha^2>$, respectively, as a function of temperature. One can see a rather good agreement between the two data sets. This can be easily understood by assuming that the tempone and orthoterphenyl molecules reorient by the same angle $\alpha$, so that the relation $x = l\alpha$ indeed holds, where $l \approx 1$ Å.

The neutron scattering data in Figure 8 may be approximated by two linear dependences—between 0 and 115 K and between 115 K and 243 K. It is interesting to note that the kink temperature of 115 K is consistent with the analogous kink for $< A_{XX} >$ obtained by $^{15}$N-ENDOR at 112 K (see Figure 4). This coincidence is in favor of the above suggestion that near 112 K onset of anharmonicity of the motion takes place, and the deviation from the linear dependence taking place at 243 K (that coincides with $T_g$) just implies the dynamical transition (see above), i.e., $T_d$ = 243 K.

Therefore, we state that temperature dependence of CW EPR spectra of guest spin-labeled molecules provides information on the dynamical transition in glassy materials, which is consistent with that obtained using neutron scattering. The important difference between the two techniques is that neutron scattering probes hydrogen atomic motions while CW EPR data refer to motions of the molecules as wholes. The obvious advantages of CW EPR are the much cheaper instrumentation and possibilities in the case of heterogeneous samples (like biological ones) to selectively explore different locations by introducing specifically spin probes and labels.

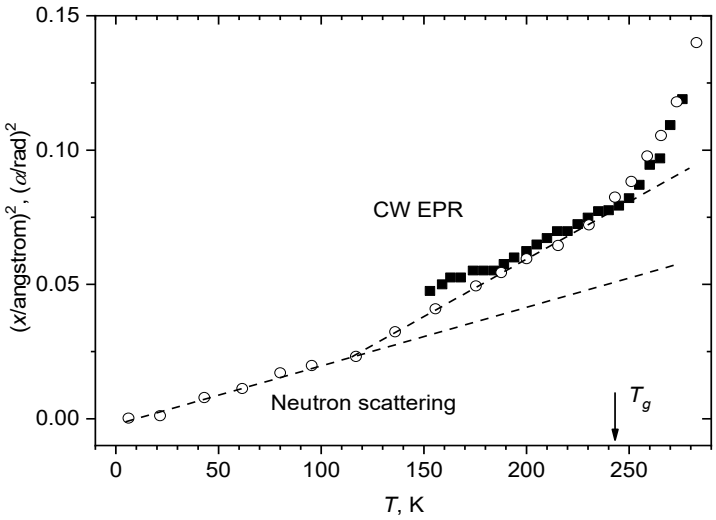


**Figure 8.** Comparison of the data for glassy *o*-terphenyl obtained by neutron scattering [87] (<$x^2$>, empty circles) and CW EPR [103] for dissolved nitroxide tempone (<$\alpha^2$>, filled squares). The two dashed straight lines show linear approximations for the neutron scattering data between 0 and 115 K and between 115 K and 243 K.

In [104], stochastic librations appearing in *o*-terphenyl glass also near 243 K were assigned to the dynamical transition as well. It is likely that the coincidence found in [104] of the onset temperatures for dynamical and stochastic librations may be a property of simple molecular glass formers; as it will be shown below, stochastic librations in complicated biological media may appear at temperatures much lower than $T_d$. And it is interesting to note that above 243 K the $< \alpha^2(t) > \tau_c$ motional parameter was found to increase with temperature remarkably faster than the <$x^2$> parameter determined from neutron scattering.

### *3.2. Cooperativity of Stochastic Librations, Influence of Hydration for Biological Systems*

In [105], stochastic librations were investigated for nitroxides of essentially different size and shape, in different solvent glasses, with different deuteration degree, and at different temperatures. There was found that the $\Delta W$ anisotropic relaxation rate (see Equation (18)) is determined by nature of the solvent glass and by temperature, and may only slightly depend on the size and shape of the nitroxide and on its deuteration. It was concluded therefore that the $\Delta W$ rate is not influenced by small angle fluctuations of the nitroxide in the stiff cage environment or by intramolecular motion in the nitroxide molecule; instead, it is induced only by repacking of the solvent cage. This implies that stochastic librations possess a cooperative nature, involving motion of the molecule surrounding. This surrounding obviously has the nanoscale size. This suggests that stochastic librations may reflect the characteristics of nanoscale molecular packing in disordered media.

This conclusion made for molecular glasses was supported in [106] for frozen lipid bilayers. In this work, stochastic librations were studied for spin-labeled amphiphilic molecules of three different kinds, embedded in bilayers of fully saturated 1,2-dipalmitoyl-*sn*-glycero-3-phosphocholine (DPPC) lipids and mono-unsaturated 1-palmitoyl-2-oleoyl-*sn*-glycero-3-phosphocholine (POPC) lipids. The spin-labeled molecules were (1) stearic acid spin-labeled by the DOXYL (4,4-dimethyl, 2-ethyl-3-oxazolidinyloxy) nitroxide radical at the 5-th carbon position (5-DSA); (2) the phospholipid 1-palmitoyl-2-oleoyl-*sn*-glycero-3-phospho(TEMPO)choline with the tempo spin label at the lipid polar head (T-PCSL); and (3) the peptide antibiotic trichogin GA IV carrying the TOAC (4-amino-1-oxyl-2,2,6,6-tetramethylpiperidine-4-carboxylic acid) spin label (TriTOAC1). For all three spin-labeled molecules investigated in [106], the similarity of the $\Delta W$ rate temperature dependences were found when these molecules were incorporated into the bilayer of the same type, DPPC or POPC. These data, however, differed remarkably for the bilayers of different types

(in more detail, see below Section 3.4). The found similarity was ascribed to the cooperative character of the ESE-detected stochastic molecular motions.

Comparison with a dry sample in [106] showed that the onset of stochastic librations is not related to lipid internal motions. Stochastic librations were also found to be suppressed for dry (lyophilized) proteins: haemoglobin [107], lysozyme [104], and casein [108].

From the other side, for lipid bilayers there was reported that motions of hydrating water and lipids are coupled [106,109]. This coupling between motions of water and biomolecules seems to be a general property of biological systems of different origins (see [28,101,110]).

### *3.3. Individual Stochastic Librations on an Inorganic Surface*

As it is shown in the previous Section 3.2, spin-labeled molecules and spin probes diluted in glassy media take part in collective motions in which their surrounding is involved. This cooperativity certainly makes the whole scenario of motions complicated because of the appearance of motional hierarchy. From this point of view, molecules adsorbed on a solid inorganic surface in diluted conditions present a pure situation when the collective effects are certainly ruled out. Indeed, an inorganic surface is much stiffer than the adsorbed organic molecule, and the mutual interactions between these molecules for their low concentration certainly can be excluded.

Motions on surfaces may occur for several reasons: (i) librations around the molecule-surface coupling bond; (ii) re-adsorption process; (iii) internal motion in the bulky molecule. In [111,112], stochastic molecular librations were investigated for different types of spin-labeled molecules adsorbed on am $SiO_2$ surface. The anisotropic relaxation rate $\Delta W$ was found to demonstrate a saturating behavior with the temperature increase, with the maximum $\Delta W_{max} \sim 1\ \mu s^{-1}$ attained near 250 K.

This saturating behavior was reproduced in simulations within a simple model of jumps by the angles $\pm\ \alpha$ between two orientations. For random jumps, ESE decays are described by the formula [113]

$$E(2\tau) = const[\,(chR\tau + \frac{w}{R}shR\tau)^2 - \frac{\Delta\omega^2}{4R^2}sh^2R\tau\,]e^{-2w\tau}, \quad (30)$$

where $w = \frac{1}{2\tau_c}$, $\Delta\omega$ is difference of the two resonance frequencies, and $R^2 = w^2 - \frac{\Delta\omega^2}{4}$. One can see that in the case of fast motion, $<\Delta\omega^2>\tau_c^2 << 1$, when also $\tau \gg \tau_c$, Equation (30) is reduced to the exponential dependence, $E(2\tau) = \exp(-2\tau\Delta\omega^2\tau_c)$, that is in full agreement with Equation (11). The advantage of this simple model is its applicability to any $\Delta\omega^2\tau_c^2$ value, i.e., this model is not restricted by the condition of fast motion that is used in the Redfield's theory of spin relaxation (see above). The saturation behavior for the $\Delta W$ temperature dependence then appears as a consequence of violation of the $<\Delta\omega^2>\tau_c^2 << 1$ condition in the Redfield's theory.

Comparison with the experiment allowed the estimation that the near temperature of the saturation (~250 K) the motional correlation time $\tau_c$ attains a value of several tens of nanoseconds, while the angle $\alpha$ is around 0.02 rad [111]. From comparison $\Delta W$ for lipid bilayers, it was concluded that the saturating behavior is an exclusive feature of the individual molecular motions. The $\Delta W_{max}$ close to the value of 1 $\mu s^{-1}$ was found in the experiment to be close for very different molecules—a small highly polar nitroxide radical and a large spin-labeled peptide—so the effect seems to be independent on the type of the molecule. Then, for any molecular system, the excess of $\Delta W > 1\ \mu s^{-1}$ may be ascribed to the effects of cooperative motions, and this excess implies that motion involves independent reorientations around several different axes.

The results of [112] showed that $\Delta W_{max}$ observed in ESE decays is enhanced for highly flexible molecules, such as stearic acid, attaining the value of 2 $\mu s^{-1}$. This effect was interpreted as a result of the two-axial (or planar) motion appearing instead of the uniaxial motion for more rigid molecules.

The results [112] also suggested that the onset of ESE-detected stochastic librational motions takes place near 130 K for systems where only molecular bending motions are expected, whereas if the molecules have enough length and intermolecular freedom for torsional motion, stochastic librations appear already at ~100 K.

This conclusion may be valid also for complex biological systems. Indeed, stochastic molecular librations for bilayers of different lipid compositions were found [106,114–117] to start either at 100 K or at 130 K – see next Section.

### *3.4. Stochastic Librations and Softness/Rigidity of Molecular Packing*

One may suggest that the weaker the intermolecular interactions, the more pronounced are cage fluctuations (see Figure 1b). Referring to the two-pulse ESE experiment on spin labels, the more effective becomes spin relaxation, the larger is the $\Delta W$ value. These expectations were nicely supported in experiments with spin-labeled lipid bilayers in their gel phase. These relatively simple systems provide several opportunities on how the intermolecular interactions can be varied. First, it can be done by variation of lipid composition in the bilayer, because fully saturated lipids are known to provide more ordered structures as compared with unsaturated lipids, so in the latter case the structures are looser and the interactions are weaker. Second, by variation the spin label location across the bilayer: for spin labels near the polar surface these interactions certainly are stronger than in the aliphatic bilayer interior, because of the electrostatic hydrogen-bond and dipolar forces in the former case. Finally, by introducing cholesterol, which, because of its well-known condensing and ordering effect on the bilayer microstructure, changes the interactions in a predicable way. Comparison of stochastic molecular librations for bilayers of different lipid compositions was performed in several works [106,114–117].

Figure 9 shows experimental results [106] for $\Delta W$ obtained in a wide temperature range in 2-pulse experiments for peptide trichogin GA IV spin-labeled with 4-amino-1-oxyl-2,2,6,6-tetramethylpiperidine-4-carboxylic acid (TOAC) nitroxide (TriTOAC1) in bilayers composed of fully saturated DPPC lipids and of mono-unsaturated POPC lipids. One can see that in the POPC bilayer the $\Delta W$ value, as compared to the DPPC bilayer, is (i) larger, (ii) starts increasing at the lower temperature (between 90 and 100 K while for the DPPC bilayer only above 130 K), and (iii) demonstrates a weaker temperature dependence. All these three features may be ascribed to the looser (softer) microstructure of the gel-phase POPC bilayer.

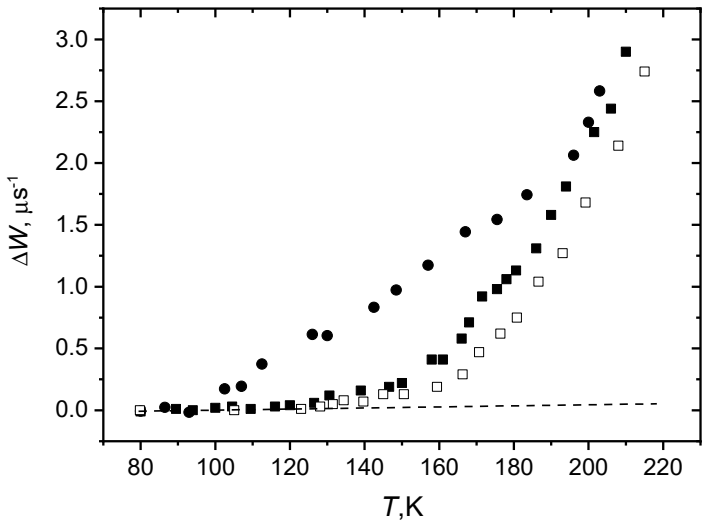


**Figure 9.** Temperature dependence of the anisotropic relaxation rate in the two-pulse experiments for TriTOAC1/POPC (filled circles), TriTOAC1/DPPC (filled squares), and T-PCSL/DPPC (open squares) bilayers. The dashed line shows the zero value. From [106] under permission, Springer.

Therefore, stochastic molecular motions here indeed serve as an indicator of the looseness (softness) of molecular parking. The coincidence of the $\Delta W$ values above 190 K in Figure 9 for both bilayers, as will be shown below, may be related to the appearance of slow rotations, i.e., with "global" softening of the matrix.

Comparison of $\Delta W$ values for spin labels located at different depths in the bilayer was done for 5-PCSL and 16-PCSL in POPC, DOPC and DPPC bilayers [114], in [116] for 5-PCSL and 16-PCSL in DPPC bilayers, for 5-DSA and 16-DSA in DPPC bilayer [117]. The results obtained for unsaturated POPC and DOPC bilayers [114] clearly demonstrated that $\Delta W$ is larger in the membrane interior, where more freedom for motion exists. For fully saturated DPPC bilayers, all the experiments showed, however, the closeness of the data for different label positions. This result for DPPC is not surprising because the DPPC molecule in the bilayer gel phase acquires an all-trans conformation [115,118], so that one may not expect dependence on the label position.

The influence of cholesterol on stochastic molecular librations in lipid bilayers was studied in [119] for POPC bilayer with T-PCSL, 5-PCSL, 10-PCSL, and 16-PCSL spin-labeled molecules. It turned out that the presence of 50 mol % of cholesterol facilitates the motions for the 16-th label position. The similar conclusion follows from comparison data in Figure 9 with the results obtained in [120]: cholesterol-free DPPC bilayer motions develop only above 130 K, while for the DPPC bilayer with 50 mol % of cholesterol [120], the motions appear already at 80 K. Motions in the membrane interior were found to be much more pronounced compared with those near the membrane surface [120]. The acceleration of motions in the presence of cholesterol was interpreted [119] as a result of freedom appearing for lipid carbon positions beyond the cholesterol core (which ends in bilayers near the 10-th carbon position of the lipid chain). This freedom unambiguously implies the weakness of intermolecular interactions, or the softness of molecular packing.

## 4. Applications

### *4.1. Dynamical Transition in Membranes and Proteins*

Biological systems are known to possess structural and dynamical properties of glassy systems [4,121,122]. For biological membranes, glass transition temperature $T_g$ was reported to be near 200 K [121,122]. Therefore, one may expect that EPR-detected dynamical transition, as it was found for simple molecular glass-formers (see Section 3.1), takes place for biological media as well.

Temperature dependence of CW EPR spectra for spin-labeled biomolecules in biological media has been studied for systems. The results are summarized in Table 1, with the dynamical transition temperatures $T_d$ indicated. (In the cases when $T_d$ was not explicitly indicated by authors, it was assessed here from the presented $<\alpha^2>$ temperature dependences).

Data in Table 1 show, first, that $T_d$ for all of the investigated membranes and proteins lies between 190 and 240 K. Second, the dynamical transition is a property of only hydrated biosystems, for lyophilized samples it disappears. And finally, for membranes it is possible to indicate the relationship between the quantitative $T_d$ value and the obvious qualitative stiffness/cohesion characteristic of the molecular packing: both characteristics are larger for the label positioned closer to the membrane surface (5-PCSL as compared to 16-PCSL, e.g.), for the membranes with more ordered lipid conformation (DPPC as compared to POPC), for the case of interdigitated lipid chains (DHPC as compared in [128] with DPPC).

The dynamical transition temperatures $T_d$ in Table 1 are in general agreement with those found by neutron scattering in purple membranes ($T_d$ = 230 K [130] and $T_d$ = 260 K [131]), in 1,2-dimyristoyl-sn-glycero-3-phosphocholine (DMPC) bilayer ($T_d$ = 250 K) [132], in DPPC bilayer ($T_d$ = 230 K) [133], in model membranes by Raman spectroscopy [118] and by differential scanning calorimetry [122].

One may then suggest that $T_d$ derived from the temperature dependence of CW EPR spectra may serve as a quantitative measure of the stiffness/cohesion of the molecular packing. The comparison of $T_d$ data for proteins lysozyme and casein [108] show that for

the latter protein, this characteristic is larger. (This is discussed below in Section 4.8 in more detail).

**Table 1.** Dynamical transition temperatures $T_d$ found from CW EPR spectra.

| System | Spin-Labeled Molecule | $T_d$ | Reference |
|---|---|---|---|
| DPPC/Cholesterol (50:50 mol/mol) membrane | 14-PCSL | 210 K | [120] |
| Human serum albumin | 5-DSA, 16-DSA | 210 K | [123] |
| Alamethicin (Ala) in membrane | Ala/TOAC, with different label position | 160 or 220 K, depending on the position | [124] |
| Human haemoglobin (Hb) in water | Hb/6-MSL | 200 K | [107] |
| Hb in 60% *v/v* glycerol–water | Hb/6-MSL | 210 K | |
| Hb lyophilized | Hb/6-MSL | non-detectable | |
| Human haemoglobin (Hb) | Hb/6-MSL | 210 K | [125] |
| Human serum albumin (HSA) | HAS/5-MSL | 210 K | |
| β-Lactoglobulin (β-LG) | β-LG/5-MSL | 210 K | |
| β-LG in 60% *v/v* glycerol–water | β-LG/5-MSL | 240 K | |
| Na,K-ATPase | 5-DSA (14-DSA) | 240 K (200 K) | [126] |
| Na,K-ATPase | Na,K-ATPase/5-MSL | 220 K | |
| DPPC membrane | 5-PCSL (16-PCSL) | 240 K (230 K) | [117] |
| DPPC membrane | 5-PCSL (16-PCSL) | 220 K (210 K) | [127] |
| DHPC membrane (interdigitated chains) | 5-PCSL (16-PCSL) | 240 K (230 K) | |
| POPC membrane | 5-PCSL (16-PCSL) | 240 K (210 K) | [114] |
| DOPC membrane | 5-PCSL (16-PCSL) | 240 K (190 K) | |
| DPPC/Lyso-PPC (interdigitated chains) | 5-PCSL, 16-PCSL | 220 K | [128] |
| DPPC membrane | 14-PCSL | 225 K | [129] |
| DPPC membrane (hydrated) | 4-PCSL | 240 K | |
| DPPC membrane (low hydration) | 4-PCSL | non-detectable | |
| Lysozyme | Lysozyme/IASL | 195 K | [108] |
| Casein | Casein/IASL | 235 K | |

Abbreviations: *n*-PCSL, 1-acyl-2-(*n*-doxyl)stearoyl-*sn*-glycero-3-phosphocholine; MSL, maleimido-tetramethylpyrrolidine-1-oxyl; *n*-DSA; stearic acid spin-labeled by the DOXYL (4,4-dimethyl, 2-ethyl-3-oxazolidinyloxy) nitroxide at the *n*-th carbon position; IASL, 4-(2-iodoacetamido)-TEMPO.

Stochastic librations detected in molecular glass formers via ESE decays also show the onset of mobility near $T_d$ [104,134], which may be related to dynamical transition observed in neutron scattering [106]. In biological membranes, however, this onset occurs above 130 K or even above 100 K (see Figure 9). On the other hand, one can see in Figure 9 that above 200 K, the $\Delta W$ value becomes larger than 2 $\mu s^{-1}$. In Section 3.3, it was indicated that $\Delta W \approx 2$ $\mu s^{-1}$ corresponds to the maximal rate achievable for individual motions of flexible biological molecules. Therefore, it would be reasonable to suggest that dynamical transition in the membrane corresponds to appearing of cooperative lipid motions. However, the validity of this suggestion needs further investigation.

### *4.2. Lipid Packing in Biological Membranes*

In [114,135], ESE-detected stochastic molecular librations of spin-labeled stearic acids and lipids in phospholipid bilayers were compared for bilayers composed of doubly unsaturated 1,2-dioleoyl-*sn*-glycero-3-phosphocholine (DOPC) lipids, mono-unsaturated

POPC lipids and fully saturated DPPC lipids. The structures of these phospholipids (and spin-labeled stearic acids) are given in Scheme 2.

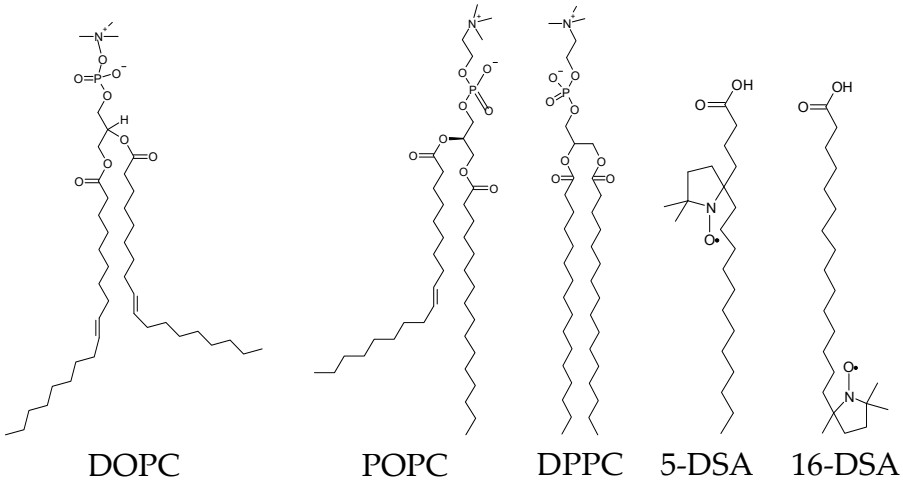


**Scheme 2.** Chemical structures of phospholipids and spin-labeled stearic acids.

For the label positions in stearic acid at the 5th and 16th carbon atoms of the acyl chain (5-DSA and 16-DSA), ESE probes motions near the membrane surface and in the membrane interior, correspondingly. As it is shown above (Section 3.4), the anisotropic contribution to the spin relaxation rate, $\Delta W$, may be used for the comparative estimation of the accessible space available for the motion. Comparison of data for the bilayers composed of lipids of a different degree of saturation of the acyl chain performed in [135] between 80 K and 210 K is shown in Figure 10.

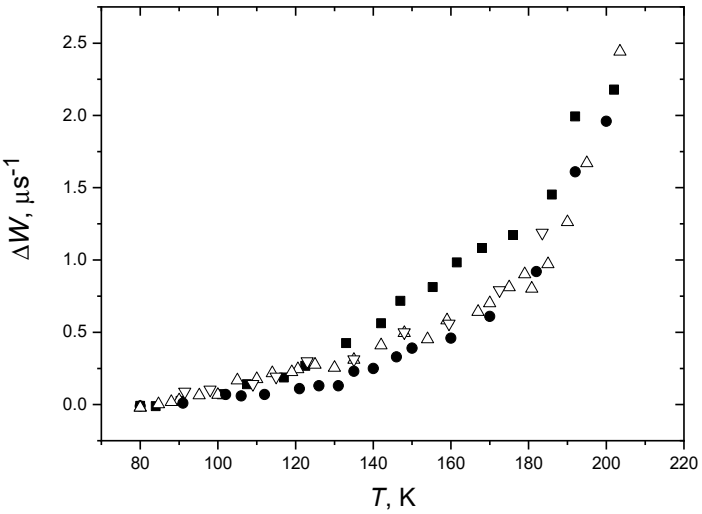


**Figure 10.** Temperature dependence of the $\Delta W$ relaxation rate obtained in two-pulse experiments for POPC/5-DSA bilayers (squares), DOPC/5-DSA bilayers (up triangles: temperature increases, down triangles: temperature decreases), for DPPC/5-DSA bilayers (circles). The experimental uncertainty is about the symbol size. From [135] under permission, Elsevier.

The data in Figure 10 show that for DOPC bilayers, the $\Delta W$ values fall between those for the POPC and DPPC bilayers. Below 130 K, it is closer to the POPC case, while above 170 K, it is closer to the DPPC case. In [135], the reversibility of the observed temperature dependences was also investigated and confirmed. The analogous results were obtained by Aloi et al. [114] in DOPC, POPC and DPPC bilayers for spin-labeled lipids 5-PCSL and 16-PCSL.

The found temperature dependence for DOPC bilayer was explained [135] by specific packing of the DOPC tails, with their terminal segments above 170 K packing cooperatively (see schematic presentation in Figure 11). At the left side here, DOPC lipids form a disordered bilayer, so the $\Delta W$ values in Figure 10 are close to those for the highly disordered POPC bilayer. On the right side, DOPC lipids form an ordered bilayer and the $\Delta W$ values are closed to that for the highly ordered DPPC bilayer.

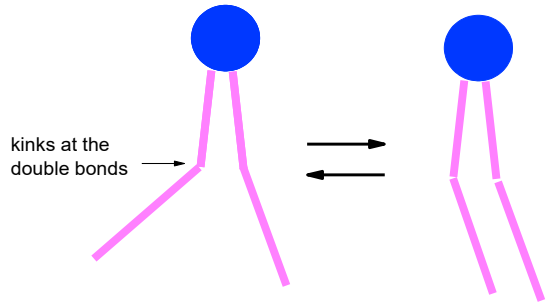


**Figure 11.** Schematic presentation of the less ordered (**left**) and more ordered (**right**) DOPC packing in the bilayer and the transition between them occurring above 120 K, which explains the results in Figure 10.

Aloi et al. [127] noticed that low-temperature librational motions found in lipid bilayers impact on the common features of glass-like behavior of biosystems, in the sense that the motion becomes pronounced at around 200 K, where the dynamical or glass transition takes place in macromolecules and supramolecular aggregates.

### *4.3. Stochastic Librations and Slow Rotations near $T_d$ in Membranes*

It is interesting to compare for biological membranes the stochastic librations and slow rotations obtained in three-pulse stimulated ESE experiment (see Section 2.4). The data plotted in a way similar to that presented in Figure 7 are shown in Figure 12 for the POPC bilayer with incorporated spin-labeled peptide Trichogin GA IV (see next Section for its detailed description). The data obey linear dependences as is predicted by Equation (29).

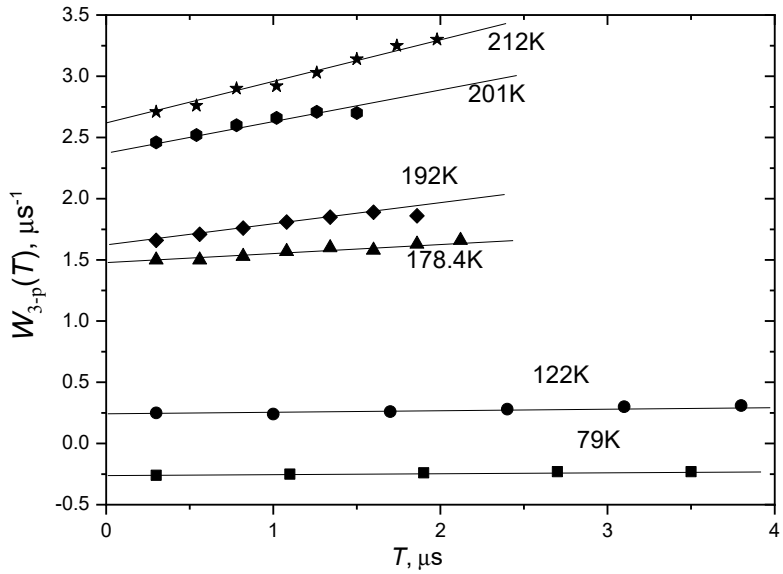


**Figure 12.** Temperature dependence of anisotropic relaxation rate obtained in three-pulse stimulated ESE experiment for POPC bilayer with incorporated spin-labeled peptide Trichogin GA IV, as a function of time delay $t_{SE}$. The straight lines show linear approximations. From [106] under permission, Springer.

Then, one can see in Figure 12 that below 190 K these dependences are approximately parallel to the horizontal axis. According to the analysis presented in Section 2.4, this means that $\tau_c < \tau$, which in turn implies that $\tau_c$ is smaller than $10^{-7}$ s. This result supports validity of the librational model of molecular motion for this system.

Above 190 K, however, the slope of the linear dependences in Figure 12 starts to increase. This increase certainly implies the appearance of slow rotations. It occurs close to the dynamical transition in this system (210 K for 16-PCSL—see Table 1). Moreover, the rate of stochastic librations detected in two-pulse ESE experiment becomes high (this rate is presented by the intercept on the vertical coordinate axis).

As it was pointed out above, slow rotations seen in three-pulse stimulated ESE experiment may be either an independent type of motion appearing at elevated temperatures or stochastic librations found in in two-pulse experiment, for which the correlation time $\tau_c$ at elevated temperatures becomes larger than $10^{-7}$ s.

### *4.4. Proteins and Antimicrobial Peptides in Membranes*

In [123], ESE was employed for investigation of interaction of human serum albumin (HAS) with the DPPC membrane. In this work, also deuterium electron spin echo envelope modulation (ESEEM) of spin-labeled stearic acids and phospholipids was used to investigate the binding of stearic acid to HSA and the adsorption of the protein on the membranes. Both the motion and the accessibility of the chains to water were found to be very different in the hydrophobic fatty acid binding sites of HSA from those in membranes.

Antimicrobial peptides (AMP) belonging to the peptaibiotic family are known for their ability to induce the permeability of biological membranes [136–140]. Peptaibiotics are characterized by the presence in the sequence of non-proteinogenic amino acid α-aminoisobutyric acid (Aib), an N-terminal acyl moiety, often an acetyl (Ac), and a C-terminal 1,2-amino alcohol (Phol). For EPR studies, Aib is replaced without loss of peptide functionality by the 4-amino-1-oxyl-2,2,6,6-tetramethylpiperidine-4-carboxylic acid (TOAC) spin label [136,139].

Alamethicin (Ala), isolated from the fungus *Trichoderma viride*, is a hydrophobic 19-amino acid peptaibiotic. In [124] spin-labeled analogs of alamethicin F50/5 [TOAC$^n$] with $n$ = 1, 8, or 16 in DMPC membrane were studied at a concentration of 1 mol %. The amino acid sequences of the three TOAC$^n$-Alm derivatives were:

Ac-**TOAC**-Pro-Aib-Ala-Aib-Ala-Glu(OMe)-Aib-Val-Aib-Gly-Leu-Aib-Pro-Val-Aib-Aib-Glu(OMe)-Glu(OMe)-Phol [TOAC$^1$]
Ac-Aib-Pro-Aib-Ala-Aib-Ala-Glu(OMe)-**TOAC**-Val-Aib-Gly-Leu-Aib-Pro-Val-Aib-Aib-Glu(OMe)-Glu(OMe)-Phol [TOAC$^8$]
Ac-Aib-Pro-Aib-Ala-Aib-Ala-Glu(OMe)-Aib-Val-Aib-Gly-Leu-Aib-Pro-Val-**TOAC**-Aib-Glu(OMe)-Glu(OMe)-Phol [TOAC$^{16}$].

Data obtained in [124] have shown that dynamical and stochastic molecular librations take place for each of the three TOAC sites, with their temperature dependence obtained in the interval between 80 and 260 K. The largest root mean squared amplitude $\sqrt{< \alpha^2 >}$ obtained from CW EPR data corresponded to 16° (for the TOAC$^8$ sample), which confirmed the used small-angle approximation. The $T_d$ values derived from CW EPR (see Table 1) were 220 K for TOAC$^1$ and TOAC$^8$ samples, and 160 K for TOAC$^{16}$. It was suggested [124] that associated with the stochastic librations the fluctuations in polar fields from the peptide could facilitate ion permeation through the membrane.

In [79] two synthetic analogues of AMP trichogin GA IV were investigated. In these analogues, one of the three Aib residues is replaced by the TOAC spin label, whereas the native C-terminal 1,2-aminoalcohol leucinol (Lol) is replaced by its synthetic precursor leucine methyl ester (Leu-OMe), and the N-terminal *n*-octanoyl (*n*Oct) group is replaced by the fluorescent (and equally hydrophobic) fluorenyl-9-methyloxycarbonyl (Fmoc) group:

*n*Oct-Aib1-Gly-Leu-Aib-Gly-Gly-Leu-Aib8-Gly-Ile-Lol (native trichogin GA IV)
Fmoc-**TOAC**1-Gly-Leu-Aib4-Gly-Gly-Leu-Aib8-Gly-Ile-Leu-OMe (FTOAC1)

Fmoc-Aib1-Gly-Leu-Aib4-Gly-Gly-Leu-**TOAC**8-Gly-Ile-Leu-OMe (FTOAC8).

It was found [79] that at a low molar peptide concentration (1:200 peptide/lipid molar ratio), the individual peptide molecules are randomly distributed at the membrane surface and spin labels demonstrate only stochastic librations in a two-pulse ESE experiment. At high peptide concentrations (1:20 ratio), slow rotations were found with a three-pulse stimulated ESE experiment. At this concentration, Trichogin GA IV is known to change its orientation from the in-plane to the transmembrane one, which is accompanied by a change from the monomeric to the dimeric state (see Figure 13). Therefore, the observed onset of slow rotations may be ascribed to the peptide dynamics around the axis parallel to the axis of lipid molecules of the membrane. Because the TOAC nitroxide spin labels are rigidly incorporated into the peptide structure, the observed mobility may be assigned to the rotation of the peptide backbone, which, in turn, might induce the transport of small polar molecules [79]. Schematically, this mechanism is shown in Figure 13.

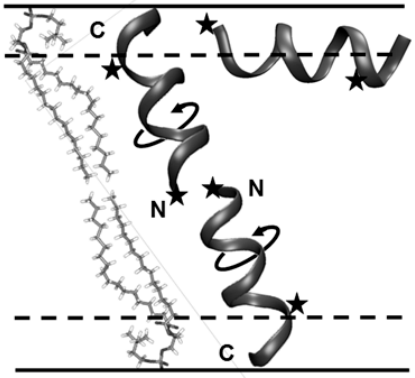


**Figure 13.** Schematic presentation of the Trichogin GA IV in-plane monomer and trans-membrane dimer and the dimer rotation in the membrane. From [79] under permission, American Chemical Society.

### *4.5. Lipid Bilayers Interacting with Cryoprotectants*

The structures of living biological objects under the extreme conditions of freezing or desiccation can be stabilized by the presence of cryoprotectants such as small sugars, sugar alcohols and others [141,142], which are accumulated by many freeze-tolerant species. For explaining molecular mechanisms of this stabilization effect, two main hypotheses are normally employed. The water replacement mechanism suggests that sugars and other cryoprotectants replace the hydration water in the biomolecules, maintaining so their polar groups at the positions close to the native ones [143–145]. Another hypothesis assumes that cryoprotectants are excluded from the hydration shell of the biomolecule and influence only the phase state of the bulk extracellular liquid [146–148]. And these opposing views were suggested to become reconciled, depending on the cryoprotectant concentration [149,150].

The studying the low-temperature motions in frozen biological systems is a promising tool for elucidation the cryoprotective mechanisms. In [117] DPPC bilayers solvated by aqueous solutions of sucrose, trehalose and sorbitol and containing incorporated 5-DSA and 16-DSA spin-labeled stearic acids were studied by two-pulse ESE. In all cases, it was found that the rate $\Delta W$ of stochastic motions increase sharply above 170–200 K. For bilayers hydrated by the sucrose and trehalose solutions, $\Delta W$ was found to increase noticeably also above ~120 K, which was explained by bilayer expanding due to direct bonding of sugar molecules to the bilayer surface. This result is in agreement with the water replacement mechanism.

The $\Delta W$ values were found to be close to those obtained for the nitroxide spin probe tempone in aqueous sorbitol and sugar glasses, which allowed to suggest that mechanism of cryoprotective action of sorbitol and sugars may also be determined by the similarity of low-temperature motions in the membrane and in the cryoprotectant-containing extracellular liquid.

In [116] stochastic motions were studied for DPPC bilayer with added spin-labeled lipids *n*-PCSL, *n* was optionally 5 or 16. Bilayers were solvated either by pure water or by 1:1 *v/v* water–glycerol mixture. For the both types of solvents and the both label positions, $\Delta W$ was found to be small below 200 K and to sharply increase above this temperature. In presence of glycerol, $\Delta W$ was found, as compared with hydration by pure water, to be larger for the 5-PCSL while for the 16-PCSL it did not change. In some experiments, a polar spin probe 3,4-dicarboxy-PROXYL was separately added to the bilayer. This probe certainly is located in the solvation shell. For 5-PCSL, the $\Delta W$ values were found to be nearly the same as those for this polar spin probe. These results indicate that lipid motions near the bilayer surface are governed by the solvating shell while motions in the bilayer interior occur independently. This conclusion was also in favor of water replacement hypothesis.

### *4.6. Supercooled Ionic Liquids*

Ionic liquids (ILs) are defined as salts with melting point below 100 °C [151–153]. Typically, ILs consist of a large asymmetric organic cation and an inorganic anion. Now ILs are attracting huge attention because of their promising scientific and technological applications, including green chemistry [154–156], nanomaterials and energy science [156–159], biomedicine [155,160], catalysis [160–162], and others. To develop these applications, elucidation of molecular self-organization properties at the nano/micro- and macroscopic scales are highly desirable [163–165].

Spin-probe EPR may appear to be a useful tool for study molecular packing in ILs. Stochastic librations in imidazolium-based ILs were studied in a series of ILs by Ivanov, Fedin and coworkers [72,166–173], using both CW and pulsed EPR. Scheme 3 presents some examples of ILs of this type and the nitroxide spin probe used.

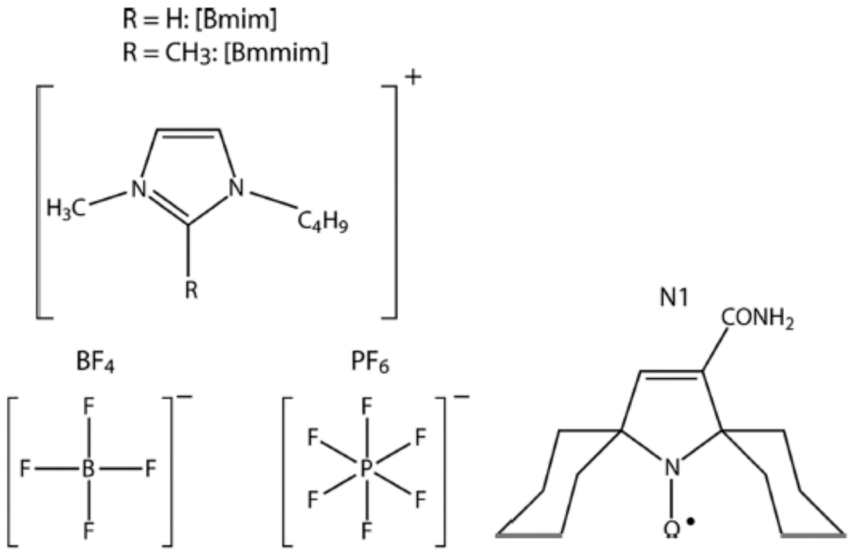


**Scheme 3.** Chemical structures of [Bmim]$PF_{4(6)}$ ILs (**left**) and nitroxide spin probe N1 (**right**).

Stochastic librations studied in a large temperature range between 20 K and 240 K has been revealed in a series of ILs in their glassy state an unusual temperature dependence near $T_g$ of the anisotropic relaxation rate $\Delta W$ (in [166–173] another denotation was used which is however coincides almost quantitatively with the $\Delta W$ rate used in this review). A typical example of the obtained temperature dependence is shown in Figure 14. The most intriguing result seen here is the drastic suppression of molecular mobility observed with temperature increase near $T_g$. This suppression implies that local density around the nanoscale spin probe solute grows with temperature, which is highly uncommon, because substances typically become less dense upon a temperature increase.

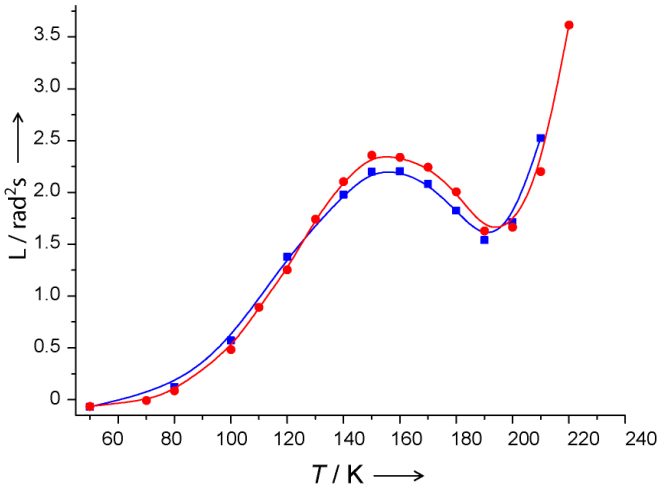


**Figure 14.** Temperature dependence of motional parameter L (that is close to the $10^6$ $\Delta W$ $s^{-1}$ value used in this review) for N1 dissolved in [Bmim]$PF_6$ (see Scheme 3). Red points correspond to the heating of the sample after shock freezing. Blue points correspond to the experiment where the sample temperature was gradually decreased starting from the room temperature. Lines represent the splines guiding the eye. $T_g$ is 197 K. From [167] under permission, American Chemical Society.

Furthermore, coexistence of two types of IL environments was observed by CW EPR [166–170] between temperatures $T_g$—60 K and $T_g$.

At first look, data in Figure 14 may reflect those mentioned above in Section 3.3 for spin-labeled molecules adsorbed on $SiO_2$ surface, which also demonstrates temperature dependence with maximum. These data were explained by large reorientation angles resulting in a violation of Redfield's theory. However, this explanation cannot be employed for IL in Figure 14. First, for ILs in Figure 14 the dependence starts at 60 K and attains its maximum at 150 K while for adsorbed molecules it starts at 100 or at 130 K and attains its maximum at 240 K, which can be easily understood as a consequence of the fact that molecules on the surface possess much more freedom of motion, which indeed results in large reorientation angles. Secondly, for ILs, the maximum in temperature dependence in Figure 14 is followed by the minimum and subsequent further increase. This effect certainly cannot be explained by large reorientation angles.

The observed unusual phenomenon in ILs was investigated by Ivanov, Fedin and coworkers in different directions. The anomaly was found to be independent of the spin probe employed—the bulky triarylmethyl probe also delivered similar information [72]. In studies of these anomalies, several EPR approaches were discovered (CW, ESE and time-resolved EPR), and the results were found to complement each other [168]. In [171], it was found that these anomalies are governed by alkyl chains of cations: for a series of ILs [$C_n$mim]$BF_4$ ($n$ = 0–12) only the chains with $n$ = 3–10 demonstrate an anomaly; moreover, remarkable even-odd $n$ dependence was found. In [172] a variety of non-IL glasses, which also contain molecules with alkyl chains, was studied. For a series of phthalates, very similar behavior to imidazolium-based ILs was clearly demonstrated, with the same length of alkyl chain.

Nanoconfinement effects on structural anomalies in imidazolium ionic liquids was studied in [170] for a series of ILs embedded into the cavities of metal–organic framework (MOF) ZIF-8. The unusual nanostructuring near $T_g$ was also observed here, and the amplitude of the anomaly was found to be dependent on the structure of the IL, thus showing the effects of molecular packing inside the MOF cavity.

In [169], binary mixtures of IL [Bmin]$BF_4$ and water were studied; it was found that water does not influence nanoclustering of IL-rich domains in which the spin probe is located. In [173], deuterated imidazolium-based ILs were compared with their protonated analogs, to assess the role of electron–nuclear spin couplings between radical probe and alkyl chains of IL; the data obtained allowed us to exclude the relaxation-induced artifacts.

### *4.7. Supercooled Deep Eutectic Solvents*

Deep eutectic solvents (DESs), first categorized by Abbott et al. in 2001 [174], are eutectic mixtures of hydrogen bond acceptors and hydrogen bond donors [175–177], with a significant freezing point depression as compared to the individual components. DESs nowadays attract considerable interest, because of their potential applications in different technological areas—metal extraction, catalysis, pharmaceuticals, green chemistry, and many others [175–177]. DESs are probably present in plants and other living systems [178].

DESs may be considered a type of ionic liquid (IL), because of the ionic nature of their components. The important difference is that ILs are synthesized and purified in relative costly technological processes; also, they may be rather toxic. On the other hand, DESs are cheap, easily prepared from broadly available components, and may belong to the green chemistry products and materials.

For broadening the DESs applications, the molecular level structural organization and structure–property relationship in DESs must be elucidated. Many DESs upon freezing can become supercooled and become a glass [179,180]. In addition, liquid DESs possess properties typical for supercooled liquids—stretched exponential relaxation, heterogeneous structural relaxations and translation−rotation decoupling [181]. Therefore, features of molecular packing found in a supercooled or glassy state may appear to be similar to those at the temperatures of their technological application.

In [182], supercooled DES consisted of choline chloride–urea (1:2) (reline), along with introduced nitroxide spin probe tempone, was studied with CW and pulsed EPR spectroscopies. In [183], these studies were extended for comparison with another DES—choline chloride–thiourea (1:2) (ChCl–thiourea). These two DESs were explored [184] as possible solvents to prepare α-chitin nanofibers (of diameter of 20–30 nm), which are used for the manufacturing of functional nanocomposites. It was found [184] that only ChCl–thiourea can be used for these purposes, so reline and ChCl-thiourea DESs certainly possess different physicochemical properties.

The data obtained [183] by CW EPR showed the coexistence of solid and liquid microphases, with assessed microviscosity of ~10 P for the liquid droplets. CW EPR spectra obtained for different temperatures showed isosbestic points for ChCl–thiourea, which indicates that these two phases are sharply separated. On the other hand, for reline, these points were found to be rather diffuse. This difference was interpreted as an indication that boundaries between two phases in reline are not so well outlined as compared to ChCl-thiourea. Data obtained with ESE showed a drastic difference for the onset of stochastic molecular librations for these two DESs, which was assigned to the higher rigidity of molecular packing for ChCl–thiourea.

It was also found that in reline the temperature dependence of stochastic molecular librations were close to that discovered for lipid bilayers [106] and globular proteins [108]. This closeness may imply the similarity of molecular packing in reline and in biological systems. It is likely that this similarity may be useful for the problems of drug delivering in living organisms and searching biocompatible DESs, which are considered to be challenging tasks nowadys [185–188].

### *4.8. Intrinsically Disordered Proteins*

For more than a century, a well-defined three-dimensional structure of a protein was considered as determining various protein functions and disfunctions in living organisms [189]. However, it was found at the turn of the 21st century [189,190] that some proteins possess significant unstructured regions, being nevertheless biologically active. These proteins were called intrinsically disordered proteins (IDPs). During the last two decades their structure and functions were intensively studied [191–197]. The intriguing property found for IDPs is their ability for disorder-to-order transitions upon target binding, when protein residues adopt specific structures upon interaction with a binding partner [191–197].

In [108], IDP bovine casein (the main proteins of milk, belonging to phosphorylated proteins) was studied with CW and pulsed EPR. For comparison, a globular pro-

tein, a hen egg white lysozyme was also investigated. Both proteins were labeled by 4-(2-iodoacetamido)-TEMPO spin label (IASL). Information on the spin label location in proteins was obtained in three-pulse stimulated electron spin echo envelope modulation (ESEEM) experiments on $D_2O$-hydrated biological systems [198]; it was concluded that spin labels are located on the peptide surface, directly exposing to the water. The hydration level $h$ used was 0.4 g of water per gram of casein ($h = 0.4$); for this level, proteins are known to be enveloped with a water monolayer [199]. For comparison purposes, dry proteins were investigated as well.

From CW EPR, the $< \alpha^2 >$ values for dynamical librations (see Sections 2.2 and 3.1) were found; the results are presented in Figure 15. One can see that below 195 K for lysozyme and below 235 K for casein, the $< \alpha^2 >$ temperature dependencies may be approximated with straight lines, which is in agreement with the model of harmonic librations. At higher temperatures, however, a noticeable deviation from the linear dependencies appear, at 195 ± 5 K for lysozyme and at 235 ± 5 K for casein. This deviation may be considered an indication on the dynamical transition.

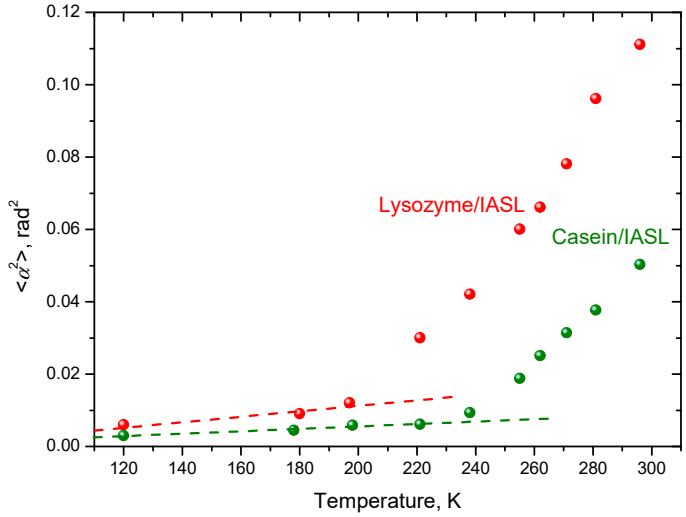


**Figure 15.** Temperature dependencies of the $< \alpha^2 >$ mean squared angular amplitudes for the dynamical librations. From [108].

The $\Delta W$ data, obtained from ESE study [108], are presented in Figure 16 as functions of temperature. For convenience of discussion, data are grouped in pairs: dehydrated and hydrated proteins (a and b), hydrated proteins (c), and dehydrated proteins (d). Data in Figure 16a,b show that for both spin-labeled proteins in their hydrated states the $\Delta W$ value increases faster than that for the dehydrated states. Therefore, molecular motions in hydrated proteins are more intensive than in dehydrated ones. Figure 16d shows that both dehydrated proteins demonstrate close temperature dependencies, which may imply proximity of their intermolecular packings.

The main result is presented in Figure 16c in which it is seen that $\Delta W$ temperature dependencies for the two hydrated proteins are essentially different. First, in casein/IASL the motions appear above 100 K, while in lysozyme/IASL they only appear above 130 K. This fact implies that in casein there is more freedom available for molecular reorientations, which is expected for their disordered structure. Secondly, for casein/IASL, a kink in the temperature dependence near 120 K appears, with remarkable slowing down above this temperature.

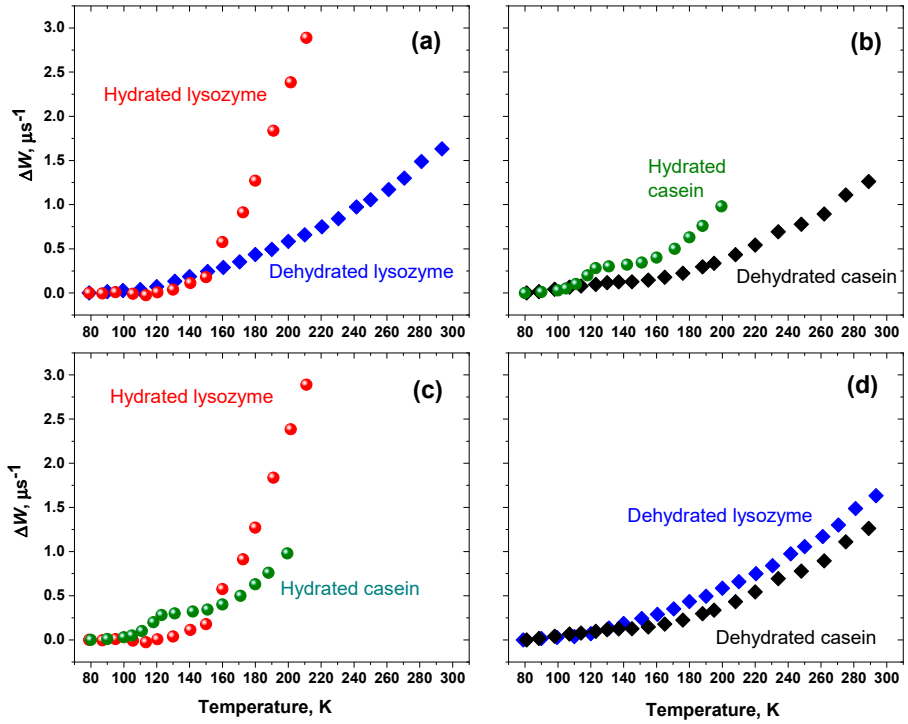


**Figure 16.** Temperature dependencies of the anisotropic relaxation rate $\Delta W$ for lysozyme/IASL and casein/IASL: (**a**,**b**) dehydrated and hydrated proteins; (**c**) hydrated proteins; (**d**) dehydrated proteins. From [108].

The explanation of this latter non-trivial effect could be as follows. As stochastic molecular librations are governed by the surrounding of the molecule (see Section 3.4), the kink at 120 K indicates that intermolecular packing in IDP casein is rearranged, providing the protein structure to become more cohesive and/or more rigid, compared with the globular protein lysozyme. The analogy could be seen here with the kink observed for the gel-phase DOPC bilayer in Figure 10. The schematic presentation of the molecule repacking given in Figure 11 for DOPC molecules may also be applicable here for casein.

As in the dehydrated state, two proteins show similar temperature dependences (see Figure 16d), then the observed rearrangement at 120 K for casein may be considered as an intrinsic property of its hydrated state—when protein possess its functionality.

### *4.9. Molecular Glasses and Other Systems*

In Sections 2.2 and 2.3, some results obtained for spin probe-dissolved molecular glass formers (o-terphenyl, glycerol) were discussed. In [44], the $A'_{ZZ}$ temperature dependences obtained by CW EPR for different molecular glasses—glycerol, water-glycerol mixture (15:85 $w/w$), trehalose, dibutyl phthalate, squalene—were obtained. The results are reproduced here in Figure 17. One can see that at low temperatures the dependences are linear, which is in agreement with Equations (7) and (8). Above $T_g$, in all the cases the linearity is broken. As it was pointed out in Section 3.1, this departure from the linearity is related to dynamical transition, which occurs at temperature $T_d$. One can further see from Figure 17 that $T_d$ in molecular glasses is close to $T_g$ (with probably one exception for the water–glycerol mixture).

The straight lines in Figure 17 possess different slopes for different types of glass. Data in [44] for different nitroxides in dibutyl phthalate also showed that the slope does not depend on the type of nitroxide, with its molecular size varying in a large interval. Note that the slope tangents in Figure 17 seem to correlate with the strength of intermolecular bonds: the slopes are smallest for glycerol and water–glycerol mixture, for which intermolecular interactions are strengthened by hydrogen bonding. In other glasses (trehalose, dibuthyl

phthalate, squalane), molecules are bonded via relatively weak van der Waals interactions, and trehalose and dibuthyl phthalate molecules, because of the polarity, interact stronger as compared with nonpolar squalane molecules. Then, the strength of intermolecular bonding results in rigidity of the potential well for librations, changing so frequency $\Omega_{\text{libr}}$ in Equation (8). Moreover, as mentioned above, the slopes of the straight lines in Figure 17 correlate with the "fragility" [45] of the glass: glycerol is known to be "strong" glass, which is commonly attributed to the network of hydrogen bonds, and it possesses the smallest slope.

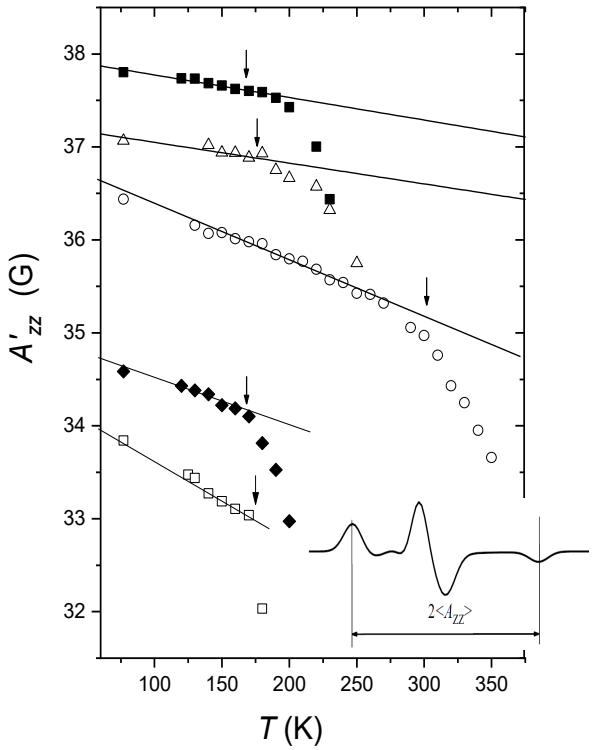


**Figure 17.** Temperature dependence of the $A'_{ZZ}$ principal value obtained from the splitting between two outer peaks in the CW EPR spectra (see insert) for nitroxide spin probes in molecular glasses: per-deuterated tempo in water–glycerol (15:85 $w/w$) mixture (filled squares), per-deuterated tempo in glycerol (empty triangles), tempone in trehalose (empty circles), per-deuterated tempo in dibutyl phthalate (rhombs), per-deuterated tempo in squalane (empty squares). The straight lines are the best fits to the experimental points in the low-temperature ranges. The arrows indicate $T_g$ s. Adapted from [44] under permission, American Institute of Physics.

Temperature dependence of ESE-detected stochastic librations of nitroxide spin probes were studied also in molecular glasses of *o*-terphenyl [104], squalane [166,167], dimethyl phthalate, diethyl phthalate, dibutyl phthalate, dioctyl phthalate [172], and sucrose octaacetate [167]. The onset of the motions for *o*-terphenyl [104] was found to coincide with $T_g$; however, for all other glasses, the motions were found to start well below $T_g$.

In [73], the dynamics of Cu(II) terpyridine complexes in ethanol glass was investigated. ESE-detected stochastic molecular librations were found also in other molecular systems: frozen photosynthetic reaction centers [67–69,200,201], polymers [202], for molecules confined in nanocapsules [71], in inclusion compounds [74], and in nanochannels [203]. In these studies, information was obtained on the orientation of the molecular axes in their environment.

These motions were found also for spin probes in living seeds and pollen [204,205]; it was suggested that the detection of these motions may serve as a measure of possible vitrification of the living objects.

*4.10. NMR of Small-Angle Motions, Secondary Relaxation*

$^2$H NMR solid-echo spectra in molecular glasses are anisotropically broadened, similarly to the CW EPR spectra. These spectra deliver information on quadrupolar coupling constant, which depends on temperature [206] analogously to the $A'_{ZZ}$ temperature dependence in CW EPR (cf. Figure 17). The change of quadrupolar constant as a function of temperature was investigated for glassy toluene-$d_5$, etanol-$d_5$, polybutadien-$d_6$, and some deuterated mixtures [206]. This dependence was attributed to dynamical librations, within a cone model [207] of fast librations. The $<\alpha^2(t)>$ temperature dependence was obtained from the quadrupolar coupling constant [206] with the relation similar to Equation (7) for CW EPR.

Stochastic molecular librations in molecular glasses were also detected with $^2$H NMR solid-echo spectra, with the time delay between two pulses sequentially increasing [32,33,206,208–210]. For these spectra, similar behavior, as for the echo-detected EPR spectra, was found: for canonical orientations, the motion-induced relaxation is slowest. The data were simulated [32] by the model of stochastic motion within a cone with a full opening angle of 6°. Therefore, $^2$H NMR is also sensitive to small-angle motions. The spectral anisotropy in $^2$H NMR is ~5 $10^5$ rad/s that is ~200 times smaller than that in EPR of nitroxide spin probes (~$10^8$ rad/s), so the typical time delays between two echo-forming pulses, for which spectral distortions are seen [32,33,206,208–210], are also ~200 time larger than in Figures 5 and 6 for ESE of nitroxides.

This behavior of $^2$H NMR solid-echo spectra was attributed [32,33,206,208–210] to the manifestation of small-angule stochastic motions (analogous experiments can be also performed employing $^{31}$P Hahn echo [209]). The results of these studies in molecular glassy systems were discussed in terms of Johari–Goldstein secondary $\beta$-relaxation process (see Introduction).

We note that ESE-detected stochastic molecular librations of spin probes and labels may hardly be related to secondary $\beta$-relaxation. Indeed, the correlation time of these librations definitely lie in the nanosecond time scale, while $\beta$-relaxation in glasses and supercooled liquids belong to the microsecond time scale [23–26]. Then, a study of magnetization transfer (MT) in a double electron–electron resonance (DEER) experiment on $^{15}$N-substituted nitroxide spin probes in molecular glasses and supercooled liquids [54,55] have shown that this MT-DEER experiment is most likely related to large-angle motions, and in this connection it was shown [55] that the observed MT effect is induced by secondary $\beta$-relaxation.

In addition, data [103] obtained for *o*-terphenyl glass with two different nitroxides dissolved—tempone and phenyl-imidasoline—have shown that while both of them similarly manifest stochastic librations, the results of the MT-DEER experiment are quite different: the MT effect is large for tempone and almost absent for phenyl-imidasoline. The absence of the MT effect in the latter case can be understood by assuming a stacking interaction between the guest phenyl-imidasoline and the host o-terphenyl molecules: this interaction artificially enlarges the guest molecule size, which in line with the results obtained in [55] would suppress secondary $\beta$-relaxation. Therefore, we may conclude that ESE-detected stochastic small-angle motions of guest spin probe molecules and molecular motions responsible for secondary $\beta$-relaxation most likely belong to different types of molecular motions.

## 5. Concluding Remarks

The elucidation of structure and dynamics of disordered media remains a very challenging problem. Comprehensive theoretical description of these systems still does not exist. It is obvious only that the core of the problem lies in mutual intermolecular interactions and/or in a nanoscale arranging of molecules. On the other hand, direct experimental means for studying properties of this arrangement are rather limited. Therefore, indirect methods may become valuable. Studying the small-angle motions of spin-labeled molecules

with EPR spectroscopy provides such an indirect tool, which allows making some definite conclusions on features of molecular packing and molecular motions in these media.

In this review, EPR applications were considered for gel-phase lipid bilayers, for biological membranes interacting with proteins, peptides and cryoprotectants, for supercooled ionic liquids and supercooled deep eutectic solvents, for globular proteins and intrinsically disordered proteins. CW EPR allows detection of dynamical transition, known for biological systems from neutron scattering experiments. The obvious advantage of CW EPR is the possibility in the case of heterogeneous samples to selectively explore different desired locations in the matter, by introducing specifically spin probes and labels. Also it is demonstrated here that appearance of ESE-detected stochastic librations reflects the softness/rigidity of the nearest molecular surrounding in these media and allows elucidating some features of their nanostructural arrangements.

**Funding:** This research was funded by the Russian Science Foundation, grant # 21-13-00025.

**Institutional Review Board Statement:** Not applicable.

**Informed Consent Statement:** Not applicable.

**Data Availability Statement:** Not applicable.

**Conflicts of Interest:** The author declares no conflict of interests.

## References

1. Paul, W.; Smith, G.D. Structure and dynamics of amorphous polymers: Computer simulations comared to experiment and theory. *Rep. Prog. Phys.* **2004**, *67*, 1117–1185. [CrossRef]
2. Saragi, T.P.I.; Spehr, T.; Siebert, A.; Fuhrmann-Lieker, T.; Salbeck, J. Spiro compounds for organic optoelectronics. *Chem. Rev.* **2007**, *107*, 1011–1065. [CrossRef] [PubMed]
3. Baghel, S.; Cathcart, H.; O'Reilly, N.J. Polymeric amorphous solid dispersions: A review of amorphization, crystallization, stabilization, solid-state characterization, and aqueous solubilization of biopharmaceutical classification system class II drugs. *J. Pharm. Sci.* **2016**, *105*, 2527–2544. [CrossRef] [PubMed]
4. Robustelli, P.; Piana, S.; Shaw, D.E. Developing a molecular dynamics force field for both folded and disordered protein states. *Proc. Natl. Acad. Sci. USA* **2018**, *115*, E4758–E4766. [CrossRef]
5. Zeller, R.C.; Pohl, R.O. Thermal conductivity and specific heat of noncrystalline solids. *Phys. Rev. B* **1971**, *4*, 2029. [CrossRef]
6. Hunklinger, S.; Arnold, W. *Ultrasonic Properties of Glasses at Low Temperatures*; Academic Press: Cambridge, MA, USA, 1976; pp. 155–215.
7. Pohl, R.O.; Liu, X.; Thompson, E. Low-temperature thermal conductivity and acoustic attenuation in amorphous solids. *Rev. Mod. Phys.* **2002**, *74*, 991–1013. [CrossRef]
8. Phillips, W.A. Tunneling states in amorphous solids. *J. Low Temp. Phys.* **1972**, *7*, 351–360. [CrossRef]
9. Anderson, P.W.; Halperin, B.I.; Varma, C.M. Anomalous low-temperature thermal properties of glasses and spin glasses. *Philos. Mag.* **1972**, *25*, 1–9. [CrossRef]
10. Phillips, W.A. Amorphous Solids: Low-Temperature Properties. In *Current Physics 24*; Springer: Berlin/Heidelberg, Germany, 1981.
11. Buchenau, U.; Nücker, N.; Dianoux, A.J. Neutron scattering study of the low-frequency vibrations in vitreous silica. *Phys. Rev. Lett.* **1984**, *53*, 2316–2319. [CrossRef]
12. Malinovsky, V.K.; Novikov, V.N.; Sokolov, A.P. Log-normal spectrum of low-energy vibrational excitations in glasses. *Phys. Lett. A* **1991**, *153*, 63–66. [CrossRef]
13. Lubchenko, V. Low-temperature anomalies in disordered solids: A cold case of contested relics? *Adv. Phys. X* **2018**, *3*, 1510296. [CrossRef]
14. Lerner, E.; Bouchbinder, E. Low-energy quasilocalized excitations in structural glasses. *J. Chem. Phys.* **2021**, *155*, 200901. [CrossRef]
15. Karpov, V.G.; Klinger, M.I.; Ignatiev, P.N. Atomic tunneling states and low-temperature anomalies of thermal properties in amorphous materials. *Solid State Commun.* **1982**, *44*, 333–337. [CrossRef]
16. Galperin, Y.M.; Karpov, V.G.; Kozub, V.I. Localized states in glasses. *Adv. Phys.* **1989**, *38*, 669–737. [CrossRef]
17. Buchenau, U. Soft localized vibrations in glasses and undercooled liquids. *Philos. Mag. B* **1992**, *65*, 303–315. [CrossRef]
18. Gurevich, V.L.; Parshin, D.A.; Pelous, J.; Schober, H.R. Theory of low energy Raman scattering in glasses. *Phys. Rev. B* **1993**, *48*, 16318–16331. [CrossRef]
19. Khodadadi, S.; Sokolov, A.P. Protein dynamics: From rattling in a cage to structural relaxation. *Soft Matter.* **2015**, *11*, 4984–4998. [CrossRef]
20. Leporini, D.; Schädler, V.; Wiesner, U.; Spiess, H.W.; Jeschke, G. Electron spin relaxation due to small-angle motion: Theory for the canonical orientations and application to hierarchic cage dynamics in ionomers. *J. Chem. Phys.* **2003**, *119*, 11829–11846. [CrossRef]
21. Bogdanov, A.V.; Vorobiev, A.K. Orientation order and rotation mobility of nitroxide biradicals determined by quantitative simulation of EPR spectra. *Phys. Chem. Chem. Phys.* **2016**, *18*, 31144–31153. [CrossRef]

22. Vorobiev, A.K.; Bogdanov, A.V.; Yankova, T.S.; Chumakova, N.A. Spin probe determination of molecular orientation distribution and rotational mobility in liquid crystals: Model-free approach. *J. Phys. Chem. B* **2019**, *123*, 5875–5891. [CrossRef]
23. Johari, G.P.; Goldstein, M.J. Viscous liquids and the glass transition. II. Secondary relaxations in glasses of rigid molecules. *Chem. Phys.* **1970**, *53*, 2372–2389. [CrossRef]
24. Johari, G.P. Intrinsic mobility of molecular glasses. *J. Chem. Phys.* **1973**, *58*, 1766–1771. [CrossRef]
25. Ngai, K.L.; Paluch, M. Classification of secondary relaxation in glass-formers based on dynamic properties. *J. Chem. Phys.* **2004**, *120*, 857–873. [CrossRef] [PubMed]
26. Gainaru, C.; Böhmer, R.; Kahlau, R.; Rössler, E. Energy landscape in molecular glasses probed by high-resolution dielectric experiments. *Phys. Rev. B* **2010**, *82*, 104205. [CrossRef]
27. Parak, F.G. Proteins in action: The physics of structural fluctuations and conformational changes. *Curr. Opin. Struct. Biol.* **2003**, *13*, 552–557. [CrossRef]
28. Doster, W. The protein-solvent glass transition. *Biochim. Biophys. Acta* **2010**, *1804*, 3–14. [CrossRef]
29. Schiró, G. Anharmonic onsets in polypeptides revealed by neutron scattering: Experimental evidences and quantitative description of energy resolution dependence. *Biophys. Chem.* **2013**, *180*, 29–36. [CrossRef]
30. Böhmer, R.; Chamberlin, R.V.; Diezemann, G.; Geil, B.; Heuer, A.; Hinze, G.; Kuebler, S.C.; Richert, R.; Schiener, B.; Sillescu, H.; et al. Nature of the non-exponential primary relaxation in structural glass-formers probed by dynamically selective experiments. *J. Non-Cryst. Solids* **1998**, *235*, 1–9. [CrossRef]
31. Ediger, M.D. Spatially heterogeneous dynamics in supercooled liquids. *Annu. Rev. Phys. Chem.* **2000**, *51*, 99–128. [CrossRef]
32. Vogel, M.; Rössler, E.A. Slow β process in simple organic glass formers studied by one- and two-dimensional $^{2}$H nuclear magnetic resonance. I. *J. Chem. Phys.* **2001**, *114*, 5802. [CrossRef]
33. Vogel, M.; Medick, P.; Rössler, E.A. Secondary relaxation processes in molecular glasses studied by nuclear magnetic resonance spectroscopy. *Annu. Rep. NMR Spectrosc.* **2005**, *56*, 231–299. [CrossRef]
34. Götze, W. Recent tests of the mode-coupling theory for glassy dynamics. *J. Phys. Condens. Matter* **1999**, *11*, A1–A45. [CrossRef]
35. Ishii, K.; Nakayama, H. Structural relaxation of vapor-deposited molecular glasses and supercooled liquids. *Phys. Chem. Chem. Phys.* **2014**, *16*, 12073–12092. [CrossRef]
36. Novikov, V.N.; Sokolov, A.P.; Strube, B.; Surovtsev, N.V.; Duval, E.; Mermet, A. Connection between quasielastic Raman scattering and free volume in polymeric glasses and supercooled liquids. *J. Chem. Phys.* **1997**, *107*, 1057. [CrossRef]
37. Goldman, S.A.; Bruno, G.V.; Polnaszek, C.F.; Freed, J.H. An ESR study of anisotropic rotational reorientation and slow tumbling in liquid and frozen media. *J. Chem. Phys.* **1972**, *56*, 716. [CrossRef]
38. Millhauser, G.L.; Freed, J.H. Two-dimensional electron spin echo spectroscopy and slow motions. *J. Chem. Phys.* **1984**, *81*, 37–48. [CrossRef]
39. Dzuba, S.A.; Maryasov, A.G.; Salikhov, K.M.; Tsvetkov, Y.D. Superslow rotations of nitroxide radicals studied by pulse EPR spectroscopy. *J. Magn. Reson.* **1984**, *58*, 95–117. [CrossRef]
40. Saxena, S.; Freed, J.H. Two-dimensional electron spin resonance and slow motions. *J. Phys. Chem. A* **1997**, *101*, 7998–8008. [CrossRef]
41. Marsh, D. *Spin-Label Electron Paramagnetic Resonance Spectroscopy*; CRC Press: Boca Raton, FL, USA, 2020. [CrossRef]
42. Van, S.P.; Birrell, G.B.; Griffith, O.H. Rapid anisotropic motion of spin labels. Models for motion averaging of the ESR parameters. *J. Magn. Reson.* **1974**, *15*, 444–459. [CrossRef]
43. Kulik, L.V.; Rapatsky, L.L.; Pivtsov, A.V.; Surovtsev, N.V.; Adichtchev, S.V.; Grigor'ev, I.A.; Dzuba, S.A. Electron-nuclear double resonance study of molecular librations of nitroxides in molecular glasses: Quantum effects at low temperatures, comparison with low-frequency Raman scattering. *J. Chem. Phys.* **2009**, *131*, 064505. [CrossRef]
44. Paschenko, S.V.; Toropov, Y.V.; Dzuba, S.A.; Tsvetkov, Y.D.; Vorobiev, A.K. Temperature dependence of amplitudes of libration motion of guest spin probe molecules in organic glasses. *J. Chem. Phys.* **1999**, *110*, 8150–8154. [CrossRef]
45. Angell, C.A. Relaxation in liquids, polymers and plastic crystals—Strong fragile patterns and problems. *J. Non-Cryst. Solids* **1991**, *131*, 13–31. [CrossRef]
46. Pivtsov, A.V.; Kulik, L.V.; Surovtsev, N.V.; Adichtchev, S.V.; Kirilyuk, I.A.; Grigor'ev, I.A.; Fedin, M.V.; Dzuba, S.A. Temperature dependence of hyperfine interaction for a $^{15}$N-nitroxide in a glassy matrix at 10–210 K. *Appl. Magn. Reson.* **2011**, *41*, 411–429. [CrossRef]
47. Dzuba, S.A.; Tsvetkov, Y.D.; Maryasov, A.G. Echo-induced EPR spectra of nitroxides in organic glasses: Model of molecular orientational motion near equilibrium position. *Chem. Phys. Lett.* **1992**, *188*, 217–222. [CrossRef]
48. Dzuba, S.A. Echo-induced EPR spectra of nitroxides: Study of molecular librations. *Pure Appl. Chem.* **1992**, *64*, 825–831. [CrossRef]
49. Kirilina, E.P.; Dzuba, S.A.; Maryasov, A.G.; Tsvetkov, Y.D. Librational dynamics of nitroxide molecules in a molecular glass studied by echo-detected EPR. *Appl. Magn. Reson.* **2001**, *21*, 203–221. [CrossRef]
50. Klauder, J.R.; Anderson, P.W. Spectral diffusion decay in spin resonance experiments. *Phys. Rev.* **1962**, *125*, 912–932. [CrossRef]
51. Abragam, A. *The Principles of Nuclear Magnetism*; Clarendon Press: Oxford, UK, 1961.
52. Dzuba, S.A. Librational motion of guest spin probe molecules in glassy media. *Phys. Lett. A* **1996**, *213*, 77–84. [CrossRef]
53. Dzuba, S.A. Librational motion of guest spin probe molecules in organic glasses: CW EPR and electron spin echo study. *Spectrochim. Acta A* **2000**, *56*, 227–234. [CrossRef]
54. Dzuba, S.A.; Tsvetkov, Y.D. Magnetization transfer in pulsed EPR of N nitroxides: Reorientational motion model of molecules in glassy liquids. *Chem. Phys.* **1988**, *120*, 291–298. [CrossRef]

55. Isaev, N.P.; Dzuba, S.A. Nitrogen nuclear spin flips in nitroxide spin probes of different sizes in glassy *o*-terphenyl: Possible relation with $\alpha$- and $\beta$-relaxations. *J. Chem. Phys.* **2011**, *135*, 094508. [CrossRef] [PubMed]
56. Syryamina, V.N.; Dzuba, S.A. Phospholipid bilayer relaxation dynamics as revealed by the pulsed electron-electron double resonance of spin labels. *J. Chem. Phys.* **2012**, *137*, 145102. [CrossRef] [PubMed]
57. Du, J.L.; Eaton, G.R.; Eaton, S.S. Temperature, orientation, and solvent dependence of electron spin-lattice relaxation rates for nitroxyl radicals in glassy solvents and doped solid. *J. Magn. Reason. A* **1995**, *115*, 213–221. [CrossRef]
58. Sato, H.; Kathirvelu, V.; Spagnol, G.; Rajca, S.; Rajca, A.; Eaton, S.S.; Eaton, G.R. Impact of electron-electron spin interaction on electron spin relaxation of nitroxide diradicals and tetraradical in glassy solvents between 10 and 300 K. *J. Phys. Chem. B* **2008**, *112*, 2818–2828. [CrossRef] [PubMed]
59. Sato, H.; Bottle, S.E.; Blinco, J.P.; Micallef, A.S.; Eaton, G.R.; Eaton, S.S. Electron spin-lattice relaxation of nitroxyl radicals in temperature ranges that span glassy solutions to low-viscosity liquids. *J. Magn. Reson.* **2008**, *191*, 66–77. [CrossRef] [PubMed]
60. Sannikova, N.; Timofeev, I.; Bagryanskaya, E.; Bowman, M.; Fedin, M.; Krumkacheva, O. Electron spin relaxation of photoexcited porphyrin in water-glycerol glass. *Molecules* **2020**, *25*, 2677. [CrossRef]
61. Kveder, M.; Merunka, D.; Jokic, M.; Makarevic, J.; Rakvin, B. Electron spin-lattice relaxation in solid ethanol: Effect of nitroxyl radical hydrogen bonding and matrix disorder. *Phys. Rev. B* **2009**, *80*, 052201. [CrossRef]
62. Erilov, D.A.; Bartucci, R.; Guzzi, R.; Marsh, D.; Dzuba, S.A.; Sportelli, L. Echo-detected electron paramagnetic resonance spectra of spin-labeled lipids in membrane model systems. *J. Phys. Chem. B* **2004**, *108*, 4501–4507. [CrossRef]
63. Isaev, N.P.; Fedin, M.V.; Dzuba, S.A. X- and Q-band electron spin echo study of stochastic molecular librations of spin labels in lipid bilayers. *Appl. Magn. Reson.* **2013**, *44*, 133–142. [CrossRef]
64. Kirilina, E.P.; Prisner, T.F.; Bennati, M.; Endeward, B.; Dzuba, S.A.; Fuchs, M.R.; Möbius, K.; Schnegg, A. Molecular dynamics of nitroxides in glasses as studied by multifrequency EPR. *Magn. Reson. Chem.* **2005**, *43*, S119–S129. [CrossRef]
65. Savitsky, A.; Plato, M.; Möbius, K. The temperature dependence of nitroxide spin–label interaction parameters: A high-field EPR study of intramolecular motional contributions. *Appl. Magn. Reson.* **2010**, *37*, 415–434. [CrossRef]
66. Hertel, M.M.; Denysenkov, V.P.; Bennati, M.; Prisner, T.F. Pulsed 180-GHz EPR/ENDOR/PELDOR spectroscopy. *Magn. Reson. Chem.* **2005**, *43*, S248–S255. [CrossRef]
67. Rohrer, M.; Gast, P.; Möbius, K.; Prisner, T.F. Anisotropic motion of semiquinones in photosynthetic reaction centers of *Rhodobacter sphaeroides* R26 and in frozen isopropanol solution as measured by pulsed high-field EPR at 95 GHz. *Chem. Phys. Lett.* **1996**, *259*, 523–530. [CrossRef]
68. Schnegg, A.; Fuhs, M.; Rohrer, M.; Lubitz, W.; Prisner, T.F.; Möbius, K. Molecular dynamics of $QA^-$ and $QB^-$ in photosynthetic bacterial reaction centers studied by pulsed high-field EPR at 95 GHz. *J. Phys. Chem. B* **2002**, *106*, 9454–9462. [CrossRef]
69. Savitsky, A.; Möbius, K. High-field EPR. *Photosynth. Res.* **2009**, *102*, 311–333. [CrossRef]
70. Steinhoff, H.-J.; Savitsky, A.; Wegener, C.; Pfeiffer, M.; Plato, M.; Möbius, K. High-field EPR studies of the structure and conformational changes of site-directed spin labeled bacteriorhodopsin. *Biochim. Biophys. Acta* **2000**, *1457*, 253–262. [CrossRef]
71. Bagryanskaya, E.G.; Polovyanenko, D.N.; Fedin, M.V.; Kulik, L.; Schnegg, A.; Savitsky, A.; Möbius, K.; Coleman, A.W.; Ananchenko, G.S.; Ripmeester, J.A. Multifrequency EPR study of the mobility of nitroxides in solid-state calixarene nanocapsules. *Phys. Chem. Chem. Phys.* **2009**, *11*, 6700–6707. [CrossRef]
72. Kuzhelev, A.A.; Krumkacheva, O.A.; Ivanov, M.Y.; Prikhod'ko, S.A.; Adonin, N.Y.; Tormyshev, V.M.; Bowman, M.K.; Fedin, M.V.; Bagryanskaya, E.G. Pulse EPR of triarylmethyl probes: A new approach for the investigation of molecular motions in soft matter. *J. Phys. Chem. B* **2018**, *122*, 8624–8630. [CrossRef]
73. Narr, E.; Zimmermann, H.; Godt, A.; Goldfarb, D.; Jeschke, G. Structure and dynamics of copper complexes with 2,2':6', 2''-terpyridines in glassy matrices. *Phys. Chem. Chem. Phys.* **2003**, *5*, 3959–3967. [CrossRef]
74. Barbon, A.; Bortolus, M.; Brustolon, M.; Comotti, A.; Maniero, A.L.; Segre, U.; Sozzani, P. Dynamics of the triplet state of a dithiophene in different solid matrixes studied by transient and pulse EPR techniques. *J. Phys. Chem. B* **2003**, *107*, 3325–3331. [CrossRef]
75. Dzuba, S.A.; Kirilina, E.P.; Salnikov, E.S.; Kulik, L.V. Restricted orientational motion of nitroxides in molecular glasses: Direct estimation of the motional time scale basing on the comparative study of primary and stimulated electron spin echo decays. *J. Chem. Phys.* **2005**, *122*, 094702. [CrossRef] [PubMed]
76. Isaev, N.P.; Dzuba, S.A. Fast stochastic librations and slow rotations of spin labeled stearic acids in a model phospholipid bilayer at cryogenic temperatures. *J. Phys. Chem. B* **2008**, *112*, 13285–13291. [CrossRef] [PubMed]
77. Isaev, N.P.; Kulik, L.V.; Kirilyuk, I.A.; Reznikov, V.A.; Grigor'ev, I.A.; Dzuba, S.A. Fast stochastic librations and slow small-angle rotations of molecules in glasses observed on nitroxide spin probes by stimulated electron spin echo spectroscopy. *J. Non-Cryst. Solids* **2010**, *356*, 1037–1042. [CrossRef]
78. Isaev, N.P.; Syryamina, V.N.; Dzuba, S.A. Small-angle orientational motions of spin labeled lipids in cholesterol-containing bilayers studied at low temperatures by electron spin echo spectroscopy. *J. Phys. Chem. B* **2010**, *114*, 9510–9515. [CrossRef] [PubMed]
79. Syryamina, V.N.; Isaev, N.P.; Peggion, C.; Formaggio, F.; Toniolo, C.; Raap, J.; Dzuba, S.A. Small-amplitude backbone motions of the spin-labeled lipopeptide trichogin GA IV in a lipid membrane as revealed by electron spin echo. *J. Phys. Chem. B* **2010**, *114*, 12277–12283. [CrossRef]
80. Ivanisenko, N.V.; Dzuba, S.A. Molecular motion in frozen phospholipid bilayers in the presence of sucrose and sorbitol studied by the spin-echo EPR of spin labels. *Appl. Magn. Reson.* **2013**, *44*, 883–891. [CrossRef]
81. Valiev, K.A.; Ivanov, E.N. Rotational brownian motion. *Sov. Phys. Uspekhi* **1973**, *16*, 1. [CrossRef]

82. Earle, K.A.; Budil, D.E.; Freed, J.H. 250-GHz EPR of nitroxides in the slow-motional regime: Models of rotational diffusion. *J. Phys. Chem.* **1993**, *97*, 13289–13297. [CrossRef]
83. Nickels, J.D.; O'Neill, H.; Hong, L.; Tyagi, M.; Ehlers, G.; Weiss, K.L.; Zhang, Q.; Yi, Z.; Mamontov, E.; Smith, J.C.; et al. Dynamics of protein and its hydration water: Neutron scattering studies on fully deuterated GFP. *Biophys. J.* **2012**, *103*, 1566–1575. [CrossRef]
84. Nienhaus, G.U.; Frauenfelder, H.; Parak, F. Structural fluctuations in glass-forming liquids: Mössbauer spectroscopy on iron in glycerol. *Phys. Rev. B* **1991**, *43*, 3345–3350. [CrossRef]
85. Wuttke, J.; Petry, W.; Coddens, G.; Fujara, F. Fast dynamics of glass-forming glycerol. *Phys. Rev. E* **1995**, *52*, 4026–4034. [CrossRef]
86. Petry, W.; Bartsch, E.; Fujara, F.; Kiebel, M.; Sillescu, H.; Farago, B. Dynamic anomaly in the glass transition region of orthoterphenyl. *Z. Phys. B Condens. Matter.* **1991**, *83*, 175–184. [CrossRef]
87. Tölle, A.; Zimmermann, H.; Fujara, F.; Petry, W.; Schmidt, W.; Schober, H.; Wuttke, J. Vibrational states of glassy and crystalline orthoterphenyl. *Eur. Phys. J. B* **2000**, *16*, 73–80. [CrossRef]
88. Tölle, A. Neutron scattering studies of the model glass former *ortho*-terphenyl. *Rep. Prog. Phys.* **2001**, *64*, 1473–1532. [CrossRef]
89. Plazanet, M.; Schober, H. Anharmonicity in a fragile glass-former probed by inelastic neutron scattering. *Phys. Chem. Chem. Phys.* **2008**, *10*, 5723–5729. [CrossRef]
90. Surovtsev, N.V.; Malinovsky, V.K.; Boldyreva, E.V. Raman study of low-frequency modes in three glycine polymorphs. *J. Chem. Phys.* **2011**, *134*, 045102. [CrossRef]
91. Roh, J.H.; Briber, R.M.; Damjanovic, A.; Thirumalai, D.; Woodson, S.A.; Sokolov, A.P. Dynamics of tRNA at different levels of hydration. *Biophys. J.* **2009**, *96*, 2755–2762. [CrossRef]
92. Fitter, J.; Lechner, R.E.; Dencher, N.A. Interactions of hydration water and biological membranes studied by neutron scattering. *J. Phys. Chem.* **1999**, *103*, 8036–8050. [CrossRef]
93. Wood, K.; Plazanet, M.; Gabel, F.; Kessler, B.; Oesterhelt, D.; Zaccai, G.; Weik, M. Dynamics of hydration water in deuterated purple membranes explored by neutron scattering. *Eur. Biophys. J.* **2008**, *37*, 619–626. [CrossRef]
94. Tobias, D.J.; Senguptaa, N.; Tarek, M. Hydration dynamics of purple membranes. *Farad. Discuss.* **2009**, *141*, 99–116. [CrossRef]
95. Frölich, A.; Gabel, F.; Jasnin, M.; Lehnert, U.; Oesterhelt, D.; Stadler, A.; Tehei, M.; Weik, M.; Wood, K.; Zaccai, G. From shell to cell: Neutron scattering studies of biological water dynamics and coupling to activity. *Farad. Discuss.* **2009**, *141*, 117–130. [CrossRef]
96. Mamontov, E.; Sharma, V.K.; Borreguero, J.M.; Tyagi, M. Protein-style dynamical transition in a non-biological polymer and a non-aqueous solvent. *J. Phys. Chem. B* **2016**, *120*, 3232–3239. [CrossRef] [PubMed]
97. Chen, S.-H.; Liu, L.; Fratini, E.; Baglioni, P.; Faraone, A.; Mamontov, E. Observation of fragile-to-strong dynamic crossover in protein hydration water. *Proc. Natl. Acad. Sci. USA* **2006**, *103*, 9012–9016. [CrossRef] [PubMed]
98. Benedetto, A.; Kearley, G.J. Elastic scattering spectroscopy (ESS): An instrument-concept for dynamics of complex (bio-) systems from elastic neutron scattering. *Sci. Rep.* **2016**, *6*, 34266. [CrossRef] [PubMed]
99. Magazù, S.; Mezei, F.; Falus, P.; Farago, B.; Mamontov, E.; Russina, M.; Migliardo, F. Protein dynamics as seen by (quasi) elastic neutron scattering. *Biochim. Biophys. Acta B* **2017**, *1861*, 3504–3512. [CrossRef] [PubMed]
100. Chen, G.; Fenimore, P.W.; Frauenfelder, H.; Mezei, F.; Swenson, J.; Young, R.D. Protein fluctuations explored by inelastic neutron scattering and dielectric relaxation spectroscopy. *Philos. Mag.* **2008**, *88*, 3877–3883. [CrossRef]
101. Khodadadi, S.; Pawlus, S.; Roh, J.H.; Sakai, V.G.; Mamontov, E.; Sokolov, A.P. The origin of the dynamical transition in proteins. *J. Chem. Phys.* **2008**, *128*, 195106. [CrossRef] [PubMed]
102. Becker, T.; Hayward, J.A.; Finney, J.L.; Daniel, R.M.; Smith, J.C. Neutron frequency windows and the protein dynamical transition. *Biophys. J.* **2004**, *87*, 1436–1444. [CrossRef]
103. Dzuba, S.A.; Salnikov, E.S.; Kulik, L.V. CW EPR, echo-detected EPR, and field-step ELDOR study of molecular motions of nitroxides in o-terphenyl glass: Dynamical transition, dynamical heterogeneity and $\beta$ relaxation. *Appl. Magn. Reson.* **2006**, *30*, 637–650. [CrossRef]
104. Golysheva, E.A.; Shevelev, G.Y.; Dzuba, S.A. Dynamical transition in molecular glasses and proteins observed by spin relaxation of nitroxide spin probes and labels. *J. Chem. Phys.* **2017**, *147*, 064501. [CrossRef]
105. Kirilina, E.P.; Grigoriev, I.A.; Dzuba, S.A. Orientational motion of nitroxides in molecular glasses: Dependence on the chemical structure, on the molecular size of the probe, and on the type of the matrix. *J. Chem. Phys.* **2004**, *121*, 12465–12471. [CrossRef]
106. Golysheva, E.A.; de Zotti, M.; Toniolo, C.; Formaggio, F.; Dzuba, S.A. Low-temperature dynamical transition in lipid bilayers detected by spin-label ESE spectroscopy. *Appl. Magn. Reson.* **2018**, *49*, 1369–1383. [CrossRef]
107. Scarpelli, F.; Bartucci, R.; Sportelli, L.; Guzzi, R. Solvent effect on librational dynamics of spin-labelled haemoglobin by ED- and CW-EPR. *Eur. Biophys, J.* **2011**, *40*, 273–279. [CrossRef]
108. Maslennikova, N.A.; Golysheva, E.A.; Dzuba, S.A. Evidence for an ordering transition near 120 K in an intrinsically disordered protein, casein. *Molecules* **2021**, *26*, 5971. [CrossRef]
109. Syryamina, V.N.; Dzuba, S.A. Dynamical transitions at low temperatures in the nearest hydration shell of phospholipid bilayers. *J. Phys. Chem. B* **2017**, *121*, 1026–1032. [CrossRef]
110. Mamontov, E.; Chu, X.-Q. Water−protein dynamic coupling and new opportunities for probing it at low to physiological temperatures in aqueous solutions. *Phys. Chem. Chem. Phys.* **2012**, *14*, 11573–11588. [CrossRef]
111. Golysheva, E.A.; Samoilova, R.I.; De Zotti, M.; Toniolo, C.; Formaggio, F.; Dzuba, S.A. Electron spin echo detection of stochastic molecular librations: Non-cooperative motions on solid surface. *J. Magn. Reson.* **2019**, *309*, 106621. [CrossRef]

112. Golysheva, E.A.; Samoilova, R.I.; De Zotti, M.; Formaggio, F.; Gobbo, M.; Dzuba, S.A. ESE-detected molecular motions of spin-labeled molecules on a solid inorganic surface: Motional models and onset temperatures. *Appl. Magn. Reson.* **2020**, *51*, 1019–1029. [CrossRef]
113. Salikhov, K.M.; Dzuba, S.A.; Raitsimring, A.M. The theory of electron spin echo signal decay resulting from dipole-dipole interactions between paramagnetic centers in solids. *J. Magn. Reson.* **1981**, *42*, 255–276. [CrossRef]
114. Aloi, E.; Guzzi, R.; Bartucci, R. Unsaturated lipid bilayers at cryogenic temperature: Librational dynamics of chain-labeled lipids from pulsed and CW-EPR. *Phys. Chem. Chem. Phys.* **2019**, *21*, 18699–18705. [CrossRef]
115. Surovtsev, N.V.; Ivanisenko, N.V.; Kirillov, K.Y.; Dzuba, S.A. Low-temperature dynamical and structural properties of saturated and monounsaturated phospholipid bilayers revealed by Raman and spin-label EPR spectroscopy. *J. Phys. Chem. B* **2012**, *116*, 8139–8144. [CrossRef] [PubMed]
116. Konov, K.B.; Isaev, N.P.; Dzuba, S.A. Low-temperature molecular motions in phospholipid bilayers in presence of glycerol as studied by spin-echo EPR of spin labels. *Appl. Magn. Reson.* **2014**, *45*, 1117–1126. [CrossRef]
117. Konov, K.B.; Isaev, N.P.; Dzuba, S.A. Low-temperature molecular motions in lipid bilayers in the presence of sugars: Insights into cryoprotective mechanisms. *J. Phys. Chem. B* **2014**, *118*, 12478–12485. [CrossRef] [PubMed]
118. Surovtsev, N.V.; Dzuba, S.A. Conformational changes of lipids in bilayers at the dynamical transition near 200 K seen by Raman scattering. *J. Phys. Chem. B* **2009**, *113*, 15558–15562. [CrossRef]
119. Isaev, N.P.; Syryamina, V.N.; Dzuba, S.A. Influence of cholesterol on molecular motions in spin-labeled lipid bilayers observed by stimulated ESE. *Appl. Magn. Reson.* **2010**, *37*, 405–413. [CrossRef]
120. Erilov, D.A.; Bartucci, R.; Guzzi, R.; Marsh, D.; Dzuba, S.A.; Sportelli, L. Librational motion of spin-labeled lipids in high-cholesterol containing membranes from echo-detected EPR spectra. *Biophys. J.* **2004**, *87*, 3873–3881. [CrossRef]
121. Weik, M.; Lehnert, U.; Zaccai, G. Liquid-like water confined in stacks of biological membranes at 200 K and its relation to protein dynamics. *Biophys. J.* **2005**, *89*, 3639–3646. [CrossRef]
122. Shalaev, E.Y.; Zografi, G.; Steponkus, P.L. Occurrence of glass transitions in long-chain phosphatidylcholine mesophases. *J. Phys. Chem. B* **2010**, *114*, 3526–3533. [CrossRef]
123. De Simone, F.; Guzzi, R.; Sportelli, L.; Marsh, D.; Bartucci, R. Electron spin-echo studies of spin-labelled lipid membranes and free fatty acids interacting with human serum albumin. *Biochim. Biophys. Acta* **2007**, *1768*, 1541–1549. [CrossRef]
124. Bartucci, R.; Guzzi, R.; De Zotti, M.; Toniolo, C.; Sportelli, L.; Marsh, D. Backbone dynamics of alamethicin bound to lipid membranes: Spin-echo electron paramagnetic resonance of TOAC-spin labels. *Biophys. J.* **2008**, *94*, 2698–2705. [CrossRef]
125. Marsh, D.; Bartucci, R.; Guzzi, R.; Sportelli, L.; Esmann, M. Librational fluctuations in protein glasses. *Biochim. Biophys. Acta* **2013**, *1834*, 1591–1595. [CrossRef]
126. Guzzi, R.; Bartucci, R.; Esmann, M.; Marsh, D. Lipid librations at the interface with the Na, K-ATPase. *Biophys. J.* **2015**, *108*, 2825–2832. [CrossRef]
127. Aloi, E.; Oranges, M.; Guzzi, R.; Bartucci, R. Low-temperature dynamics of chain-labeled lipids in ester- and ether-linked phosphatidylcholine membranes. *J. Phys. Chem. B* **2017**, *121*, 9239–9246. [CrossRef]
128. Aloi, E.; Bartucci, R. Interdigitated lamellar phases in the frozen state: Spin-label CW- and FT-EPR. *Biophys. Chem.* **2019**, *253*, 106229. [CrossRef]
129. Aloi, E.; Bartucci, R. Influence of hydration on segmental chain librations and dynamical transition in lipid bilayers. *Biochim. Biphys. Acta-Biomembr.* **2022**, *1864*, 183805. [CrossRef]
130. Ferrand, M.; Petry, W.; Dianoux, A.J.; Zaccai, G. Dynamical transition of bacteriorhodopsin in purple membranes revealed by neutron scattering: A relation between structure, dynamics and function. *Phys. A* **1993**, *201*, 425–429. [CrossRef]
131. Wood, K.; Plazanet, M.; Gabel, F.; Kessler, B.; Oesterhelt, D.; Zaccai, G.; Weik, M. Coupling of protein and hydration-water dynamics in biological membranes. *Proc. Natl. Acad. Sci. USA* **2007**, *104*, 18049–18054. [CrossRef]
132. Peters, J.; Marion, J.; Natali, F.; Kats, E.; Bicout, D.J. The dynamical transition of lipid multilamellar bilayers as a matter of cooperativity. *J. Phys. Chem. B* **2017**, *121*, 6860–6868. [CrossRef]
133. Doxastakis, M.; Sakai, V.G.; Ohtake, S.; Maranas, J.K.; de Pablo, J.J. A molecular view of melting in anhydrous phospholipidic membranes. *Biophys. J.* **2007**, *92*, 147–161. [CrossRef]
134. Dzuba, S.A.; Kirilina, E.P.; Salnikov, E.S. On the possible manifestation of harmonic-anharmonic dynamical transition in glassy media in electron paramagnetic resonance of nitroxide spin probes. *J. Chem. Phys.* **2006**, *125*, 054502. [CrossRef]
135. Golysheva, E.A.; Dzuba, S.A. Lipid chain mobility and packing in DOPC bilayers at cryogenic temperatures. *Chem. Phys. Lipids* **2020**, *226*, 104817. [CrossRef] [PubMed]
136. Toniolo, C.; Brückner, H. (Eds.) Peptaibiotics: Fungal Peptides Containing α-Dialkyl α-Amino Acids. In *Verlag Helvetica Chimica Acta*; Zurich and Wiley-VCH: Weinheim, Germany, 2009.
137. Duclohier, H. Antimicrobial peptides and peptaibols, substitutes for conventional antibiotics. *Curr. Pharm. Des.* **2010**, *16*, 3212–3223. [CrossRef] [PubMed]
138. Bocchinfuso, G.; Palleschi, A.; Orioni, B.; Grande, G.; Formaggio, F.; Toniolo, C.; Park, Y.; Hahm, K.-S.; Stella, L. Different mechanisms of action of antimicrobial peptides: Insights from fluorescence spectroscopy experiments and molecular dynamics simulations. *J. Pept. Sci.* **2009**, *15*, 550–558. [CrossRef] [PubMed]
139. Toniolo, C.; Crisma, M.; Formaggio, F. TOAC, a nitroxide spin-labeled, achiral C(alpha)-tetrasubstituted alpha-amino acid, is an excellent tool in material science and biochemistry. *Pept. Sci.* **1998**, *47*, 153–158. [CrossRef]

140. Neumann, N.K.N.; Stoppacher, N.; Zeilinger, S.; Degenkolb, T.; Brückner, H.; Schuhmacher, R. The peptaibiotics database—A comprehensive online resource. *Chem. Biodivers.* **2015**, *12*, 743–751. [CrossRef]
141. Crowe, J.H.; Carpenter, J.F.; Crowe, L.M. The role of vitrification in anhydrobiosis. *Annu. Rev. Physiol.* **1998**, *60*, 73–103. [CrossRef]
142. Hoekstra, F.A.; Golovina, E.A.; Buitink, J. Mechanisms of plant desiccation tolerance. *Trends Plant. Sci.* **2001**, *6*, 431–438. [CrossRef]
143. Leekumjorn, S.; Sum, A.K. Molecular investigation of the interactions of trehalose with lipid bilayers of DPPC, DPPE and their mixture. *Mol. Simul.* **2006**, *32*, 219–230. [CrossRef]
144. Lairion, F.; Disalvo, E.A. Effect of trehalose on the contributions to the dipole potential of lipid monolayers. *Chem. Phys. Lipids* **2007**, *150*, 117–124. [CrossRef]
145. Golovina, E.A.; Golovin, A.; Hoekstra, F.A.; Faller, R. Water replacement hypothesis in atomic details: Effect of trehalose on the structure of single dehydrated POPC bilayers. *Langmuir* **2010**, *26*, 11118–11126. [CrossRef]
146. Koster, K.L.; Maddocks, K.J.; Bryant, G. Exclusion of maltodextrins from phosphatidylcholine multilayers during dehydration: Effects on membrane phase behavior. *Eur. Biophys. J.* **2003**, *32*, 96–105. [CrossRef]
147. Lenné, T.; Garvey, C.J.; Koster, K.L.; Bryant, G. Effects of sugars on lipid bilayers during dehydration—SAXS/WAXS measurements and quantitative model. *J. Phys. Chem. B* **2009**, *113*, 2486–2491. [CrossRef]
148. Kent, B.; Hunt, T.; Darwish, T.A.; Hauss, T.; Garvey, C.J.; Bryant, G. Localization of trehalose in partially hydrated DOPC bilayers: Insights into cryoprotective mechanisms. *J. R. Soc. Interface* **2014**, *11*, 20140069. [CrossRef]
149. Westh, P. Glucose, sucrose and trehalose are partially excluded from the interface of hydrated DMPC bilayers. *Phys. Chem. Chem. Phys.* **2008**, *10*, 4110–4112. [CrossRef]
150. Andersen, H.D.; Wang, C.; Arleth, L.; Peters, G.H.; Westh, P. Reconciliation of opposing views on membrane–sugar interactions. *Proc. Natl. Acad. Sci. USA* **2011**, *108*, 1874–1878. [CrossRef]
151. Hayes, R.; Warr, G.G.; Atkin, R. Structure and nanostructure in ionic liquids. *Chem. Rev.* **2015**, *115*, 6357–6426. [CrossRef]
152. Hallett, J.P.; Welton, T. Room-temperature ionic liquids: Solvents for synthesis and catalysis. *Chem. Rev.* **2011**, *111*, 3508–3576. [CrossRef]
153. Rogers, R.D. Chemistry: Ionic liquids–solvents of the future? *Science* **2003**, *302*, 792–793. [CrossRef]
154. Blanchard, L.A.; Hancu, D.; Beckman, E.J.; Brennecke, J.F. Green processing using ionic liquids and $CO_2$. *Nature* **1999**, *399*, 28–29. [CrossRef]
155. Egorova, K.S.; Gordeev, E.G.; Ananikov, V.P. Biological activity of ionic liquids and their application in pharmaceutics and medicine. *Chem. Rev.* **2017**, *117*, 7132–7189. [CrossRef]
156. Watanabe, M.; Thomas, M.L.; Zhang, S.; Ueno, K.; Yasuda, T.; Dokko, K. Application of ionic liquids to energy storage and conversion materials and devices. *Chem. Rev.* **2017**, *117*, 7190–7239. [CrossRef]
157. Singh, R.P.; Verma, R.D.; Meshri, D.T.; Shreeve, J.M. Energetic nitrogen-rich salts and ionic liquids. *Angew. Chem. Int. Ed.* **2006**, *45*, 3584–3601. [CrossRef] [PubMed]
158. Macfarlane, D.R.; Tachikawa, N.; Forsyth, M.; Pringle, J.M.; Howlett, P.C.; Elliott, G.D.; Davis, J.H.; Watanabe, M.; Simon, P.; Angell, C.A. Energy applications of ionic liquids. *Energy Environ. Sci.* **2014**, *7*, 232–250. [CrossRef]
159. Manthiram, A.; Fu, Y.; Chung, S.H.; Zu, C.; Su, Y.S. Rechargeable lithium-sulfur batteries. *Chem. Rev.* **2014**, *114*, 11751–11787. [CrossRef]
160. van Rantwijk, F.; Sheldon, R.A. Biocatalysis in ionic liquids. *Chem. Rev.* **2007**, *107*, 2757–2785. [CrossRef] [PubMed]
161. Giernoth, R. Task-specific ionic liquids. *Angew. Chem. Int. Ed.* **2010**, *49*, 2834–2839. [CrossRef] [PubMed]
162. Wasserscheid, P.; Keim, W. Ionic liquids—New 'solutions' for transition metal catalysis. *Angew. Chem. Int. Ed.* **2000**, *39*, 3772–3789. [CrossRef]
163. Trioli, A.; Russina, O.; Bleif, H.-J.; Di Cola, E. Nanoscale segregation in Room Temperature Ionic Liquids. *J. Phys. Chem. B* **2007**, *111*, 4641–4644. [CrossRef]
164. Weingärtner, H. Understanding ionic liquids at the molecular level: Facts, problems, and controversies. *Angew. Chem. Int. Ed.* **2008**, *47*, 654–670. [CrossRef]
165. Mogurampelly, S.; Keith, J.R.; Ganesan, V. Mechanisms underlying ion transport in polymerized ionic liquids. *J. Am. Chem. Soc.* **2017**, *139*, 9511–9514. [CrossRef]
166. Ivanov, M.Y.; Krumkacheva, O.A.; Dzuba, S.A.; Fedin, M.V. Microscopic rigidity and heterogeneity of ionic liquids probed by stochastic molecular librations of the dissolved nitroxides. *Phys. Chem. Chem. Phys.* **2017**, *19*, 26158–26163. [CrossRef]
167. Ivanov, M.Y.; Prikhod'ko, S.A.; Adonin, N.Y.; Kirilyuk, I.A.; Adichtchev, S.V.; Surovtsev, N.V.; Dzuba, S.A.; Fedin, M.V. Structural anomalies in ionic liquids near the glass transition revealed by pulse EPR. *J. Phys. Chem. Lett.* **2018**, *9*, 4607–4612. [CrossRef]
168. Ivanov, M.Y.; Fedin, M.V. Nanoscale heterogeneities in ionic liquids: Insights from EPR of spin probes. *Mendeleev Commun.* **2018**, *28*, 565–573. [CrossRef]
169. Ivanov, M.Y.; Prikhod'ko, S.A.; Adonin, N.Y.; Fedin, M.V. Structural anomalies in binary mixtures of ionic liquid [Bmim]$BF_4$ with water studied by EPR. *J. Phys. Chem. B* **2019**, *123*, 9956–9962. [CrossRef]
170. Ivanov, M.Y.; Poryvaev, A.S.; Polyukhov, D.M.; Prikhod'ko, S.A.; Adonin, N.Y.; Fedin, M.V. Nanoconfinement effects on structural anomalies in imidazolium ionic liquids. *Nanoscale* **2020**, *12*, 23480–23487. [CrossRef]
171. Bakulina, O.D.; Ivanov, M.Y.; Prikhod'ko, S.A.; Pylaeva, S.I.; Zaytseva, V.; Surovtsev, N.V.; Adonin, N.Y.; Fedin, M.V. Nanocage formation and structural anomalies in imidazolium ionic liquid glasses governed by alkyl chains of cations. *Nanoscale* **2020**, *12*, 19982–19991. [CrossRef]
172. Ivanov, M.Y.; Bakulina, O.D.; Alimov, D.V.; Prikhod'ko, S.A.; Veber, S.L.; Pylaeva, S.; Adonin, N.Y.; Fedin, M.V. Inherent heterogeneities and nanostructural anomalies in organic glasses revealed by EPR. *Nanoscale Adv.* **2021**, *3*, 4973–4978. [CrossRef]

173. Ivanov, M.Y.; Prikhod'ko, S.A.; Bakulina, O.D.; Kiryutin, A.S.; Adonin, N.Y.; Fedin, M.V. Validation of structural grounds for anomalous molecular mobility in ionic liquid glasses. *Molecules* **2021**, *26*, 5828. [CrossRef]
174. Abbott, A.P.; Capper, G.; Davies, D.L.; Munro, H.L.; Rasheed, R.K.; Tambyrajah, V. Preparation of novel, moisture-stable, lewis-acidic ionic liquids containing quaternary ammonium salts with functional side chains. *Chem. Commun.* **2001**, *19*, 2010–2011. [CrossRef]
175. Smith, E.L.; Abbott, A.P.; Ryder, K.S. Deep eutectic solvents (DESs) and their applications. *Chem. Rev.* **2014**, *114*, 11060–11082. [CrossRef]
176. Paiva, A.; Craveiro, R.; Aroso, I.; Martins, M.; Reis, R.L.; Duarte, R.C. Natural deep eutectic solvents—Solvents for the 21st century. *ACS Sustain. Chem. Eng.* **2014**, *2*, 1063–1071. [CrossRef]
177. Hansen, B.B.; Spittle, S.; Chen, B.; Poe, D.; Zhang, Y.; Klein, J.M.; Horton, A.; Adhikari, L.; Zelovich, T.; Doherty, B.W.; et al. Deep eutectic solvents: A review of fundamentals and applications. *Chem. Rev.* **2021**, *121*, 1232–1285. [CrossRef]
178. Dai, Y.; Varypataki, E.M.; Golovina, E.A.; Jiskoot, W.; Witkamp, G.-J.; Choi, Y.H.; Verpoorte, R. Chapter Seven—Natural deep eutectic solvents in plants and plant cells: In vitro evidence for their possible functions. *Adv. Botan. Res.* **2021**, *97*, 159–184. [CrossRef]
179. Reuter, D.; Munzner, P.; Gainaru, C.; Lunkenheimer, P.; Loidl, A.; Bohmer, R. Translational and reorientational dynamics in deep eutectic solvents. *J. Chem. Phys.* **2021**, *154*, 154501. [CrossRef] [PubMed]
180. Dai, Y.; van Spronsen, J.; Witkamp, G.-J.; Verpoorte, R.; Choi, Y.H. Natural deep eutectic solvents as new potential media for green technology. *Anal. Chim. Acta* **2013**, *766*, 61–68. [CrossRef] [PubMed]
181. Srinivasan, H.; Sharma, V.K.; Mukhopadhyay, R.; Mitra, S. Solvation and transport of lithium ions in deep eutectic solvents. *J. Chem. Phys.* **2020**, *153*, 104505. [CrossRef] [PubMed]
182. Golysheva, E.A.; Dzuba, S.A. Low-temperature molecular motions in a deep eutectic solvent choline chloride/urea studied by spin-probe EPR. *Russ. Chem. Bull.* **2021**, *70*, 2366–2369. [CrossRef]
183. Golysheva, E.A.; Maslennikova, N.A.; Baranov, D.S.; Dzuba, S.A. Structural properties of supercooled deep eutectic solvents: Choline chloride–thiourea compared to reline. *Phys. Chem. Chem. Phys.* 2022. [CrossRef]
184. Mukesh, C.; Mondal, D.; Sharma, M.; Prasad, K. Choline chloride-thiourea, a deep eutectic solvent for the production of chitin nanofibers. *Carbohydr. Polym.* **2014**, *103*, 466–471. [CrossRef]
185. Zainal-Abidin, M.H.; Hayyan, M.; Ngoh, G.C.; Wong, W.F.; Looi, C.Y. Emerging frontiers of deep eutectic solvents in drug discovery and drug delivery systems. *J. Control. Release* **2019**, *316*, 168–195. [CrossRef]
186. Emami, S.; Shayanfar, A. Deep eutectic solvents for pharmaceutical formulation and drug delivery applications. *Pharm. Dev. Technol.* **2020**, *25*, 779–796. [CrossRef]
187. Mbous, Y.P.; Hayyan, M.; Wong, W.F.; Hayyan, A.; Looi, C.Y.; Hashim, M.A. Simulation of deep eutectic solvents' interaction with membranes of cancer cells using COSMO-RS. *J. Phys. Chem. B* **2020**, *124*, 9086–9094. [CrossRef]
188. Wagle, D.V.; Zhao, H.; Baker, G.A. Deep eutectic solvents: Sustainable media for nanoscale and functional materials. *Acc. Chem. Res.* **2014**, *47*, 2299–2308. [CrossRef]
189. Dunker, A.; Lawson, J.D.; Brown, C.J.; Williams, R.M.; Romero, P.; Oh, J.S.; Oldfield, C.J.; Campen, A.M.; Ratliff, C.R.; Hipps, K.W.; et al. Intrinsically disordered protein. *J. Mol. Graph. Modell.* **2001**, *19*, 26–59. [CrossRef]
190. Wright, P.E.; Dyson, H. Intrinsically unstructured proteins: Reassessing the protein structure-function paradigm. *J. Mol. Biol.* **1999**, *293*, 321–331. [CrossRef]
191. Wright, P.E.; Dyson, H.J. Intrinsically disordered proteins in cellular signalling and regulation. *Nat. Rev. Mol. Cell Biol.* **2015**, *16*, 18–29. [CrossRef]
192. Uversky, V.N. Unusual biophysics of intrinsically disordered proteins. *Biochim. Biophys. Acta-Proteins Proteom.* **2013**, *1834*, 932–951. [CrossRef]
193. Oldfield, C.J.; Dunker, A.K. Intrinsically disordered proteins and intrinsically disordered protein regions. *Annu. Rev. Biochem.* **2014**, *83*, 553–584. [CrossRef]
194. Deiana, A.; Forcelloni, S.; Porrello, A.; Giansanti, A. Intrinsically disordered proteins and structured proteins with intrinsically disordered regions have different functional roles in the cell. *PLoS ONE* **2019**, *14*, e0217889. [CrossRef]
195. Drake, J.A.; Pettitt, B.M. Physical chemistry of the protein backbone: Enabling the mechanisms of intrinsic protein disorder. *J. Phys. Chem. B* **2020**, *124*, 4379–4390. [CrossRef]
196. Hosoya, Y.; Ohkanda, J. Intrinsically disordered proteins as regulators of transient biological processes and as untapped drug targets. *Molecules* **2021**, *26*, 2118. [CrossRef]
197. Uversky, V.N. Supramolecular fuzziness of intracellular liquid droplets: Liquid-liquid phase transitions, membrane-less organelles, and intrinsic disorder. *Molecules* **2019**, *24*, 3265. [CrossRef] [PubMed]
198. Milov, A.D.; Samoilova, R.I.; Shubin, A.A.; Grishin, Y.A.; Dzuba, S.A. ESEEM measurements of local water concentration in $D_2O$-containing spin-labeled systems. *Appl. Magn. Reson.* **2008**, *35*, 73–94. [CrossRef]
199. Rupley, J.A.; Careri, G. Protein hydration and function. *Adv. Protein Chem.* **1991**, *41*, 37–172. [CrossRef] [PubMed]
200. Borovykh, V.; Gast, P.; Dzuba, S.A. The dynamical transition in proteins of bacterial photosynthetic reaction centers observed by echo-detected EPR of specific spin labels. *Appl. Magn. Reson.* **2007**, *31*, 159–166. [CrossRef]
201. Möbius, K.; Savitsky, V.; Schnegg, A.; Plato, M.; Fuchs, M. High-field EPR spectroscopy applied to biological systems: Characterization of molecular switches for electron and ion transfer. *Phys. Chem. Chem. Phys.* **2005**, *7*, 19–42. [CrossRef] [PubMed]
202. Leporini, D.; Jeschke, G. Cage effects on the librational motion in ionomeric homopolymers and block copolymers. *Phil. Mag.* **2004**, *84*, 1567–1572. [CrossRef]

203. Brustolon, M.; Barbon, A.; Bortolus, M.; Maniero, A.L.; Sozzani, P.; Comotti, A.; Simonutti, R. Dynamics of Alkoxy-Oligothiophene Ground and Excited States in Nanochannels. *J. Am. Chem. Soc.* **2004**, *126*, 15512–15519. [CrossRef]
204. Dzuba, S.A.; Golovina, Y.A.; Tsvetkov, Y.D. Echo-induced EPR spectra of spin probes as a method for identification of glassy state in biological objects. *J. Magn. Reson. B* **1993**, *101*, 134–138. [CrossRef]
205. Buitink, J.; Dzuba, S.A.; Hoekstra, F.A.; Tsvetkov, Y.D. Pulsed EPR spin-probe study of intracellular glasses in seed and pollen. *J. Magn. Reson.* **2000**, *142*, 364–368. [CrossRef]
206. Böhmer, R.; Diezemann, G.; Hinze, G.; Rössler, E. Dynamics of supercooled liquids and glassy solids. *Progr. Nucl. Magn. Reson. Spectr.* **2001**, *39*, 191–267. [CrossRef]
207. Batchelor, L.S.; Niu, C.N.; Torchia, D.A. Methyl reorientation in polycrystalline amino acids and peptides: A deuteron NMR spin-lattice relaxation study. *J. Am. Chem. Soc.* **1983**, *105*, 2228–2231. [CrossRef]
208. Vogel, M.; Tschirwitz, C.; Schneider, G.; Koplin, C.; Medick, P.; Rössler, E. A $^{2}$H NMR and dielelectric spectroscopy study of the slow β-process in organic glass formers. *J. Non-Cryst. Solids* **2002**, *307*, 326. [CrossRef]
209. Pötzschner, B.; Mohamed, F.; Bächer, C.; Wagner, E.; Lichtinger, A.; Bock, D.; Kreger, K.; Schmidt, H.-W.; Rössler, E.A. Non-polymeric asymmetric binary glass-formers. II. Secondary relaxation studied by dielectric, 2H NMR, and 31P NMR spectroscopy. *J. Chem. Phys.* **2017**, *146*, 164504. [CrossRef]
210. Steinrucken, E.; Becher, M.; Vogel, M. On the molecular mechanisms of α and β relaxations in ionic liquids. *J. Chem. Phys.* **2020**, *153*, 104507. [CrossRef]